IAS SEDIMENTOLOGY
Journal of the International Association of Sedimentologists

Multiphase dolomitization of deeply buried Cambrian petroleum reservoirs, Tarim Basin, Northwest China

Journal:	*Sedimentology*
Manuscript ID	SED-2015-OM-192.R3
Manuscript Type:	Original Manuscript
Date Submitted by the Author:	08-May-2016

Complete List of Authors:	JIANG, LEI; Institute of Geology and Geophysics, Chinese Academy of Sciences; University of Liverpool, Department of Earth, Ocean and Ecological Sciences, School of Environmental Sciences; The University of Texas at Austin, Bureau of Economic Geology, Jackson School of Geosciences Cai, Chun Fang; Institute of Geology and Geophysics, Chinese Academy of Sciences; Yangtze University, Key Laboratory of Exploration Technologies for Oil and Gas Resources, Ministry of Education, School of Water Resource and Environment Worden, Richard; University of Liverpool, Department of Earth, Ocean and Ecological Sciences, School of Environmental Sciences Crowley, Stephen; University of Liverpool, Department of Earth, Ocean and Ecological Sciences, School of Environmental Sciences Jia, Lianqi; Institute of Geology and Geophysics, Chinese Academy of Sciences Zhang, Ke; Tarim Oilfield Company, PetroChina, Research Institute of Petroleum Exploration and Development Duncan, Ian; The University of Texas at Austin, Bureau of Economic Geology, Jackson School of Geosciences

Keywords:	Carbonate reservoir, dolomitization, hydrothermal fluids, fluid inclusions, C/O/Sr isotopes, restricted lagoon, Cambrian

Multiphase dolomitization of deeply buried Cambrian petroleum reservoirs, Tarim Basin, Northwest China

LEI JIANG[a,b,c*], CHUNFANG CAI [d,a*], RICHARD H. WORDEN[b], STEPHEN F. CROWLEY[b], LIANQI JIA[a], KE ZHANG[e], IAN J. DUNCAN[c]

[a]Key Laboratory of Petroleum Resources Research, Institute of Geology and Geophysics, Chinese Academy of Sciences, Beijing 100029, China

[b]Department of Earth, Ocean and Ecological Sciences, School of Environmental Sciences, University of Liverpool, Liverpool, L69 3GP, UK

[c]Bureau of Economic Geology, Jackson School of Geosciences, The University of Texas at Austin, Austin, TX 78713, United States

[d]Key Laboratory of Exploration Technologies for Oil and Gas Resources, Ministry of Education, School of Water Resource and Environment, Yangtze University, Caidian, Wuhan, Hubei 430100, PR China

[e]Research Institute of Petroleum Exploration and Development, Tarim Oilfield Company, PetroChina, Korla, Xinjiang 841000, China

*Corresponding author #1: Prof. Dr Chunfang Cai

Key Laboratory of Exploration Technologies for Oil and Gas Resources, Ministry of Education, School of Water Resource and Environment, Yangtze University, Caidian, Wuhan, Hubei 430100, PR China

Email: cai_cf@mail.iggcas.ac.cn

Telephone: 86-10-82998127; Fax: 86-10-62010846

*Corresponding author #2: Dr. Lei Jiang

Key Laboratory of Petroleum Resources Research, Institute of Geology and Geophysics, Chinese Academy of Sciences

Email: lei.jiang@mail.iggcas.ac.cn

Telephone: 86-10-82998128; Fax: 86-10-62010846

ABSTRACT

Cambrian dolostone reservoirs in the Tarim Basin, China, have significant potential for future discoveries of petroleum although exploration and production planning is hampered by limited understanding of the occurrence and distribution of dolomite in such ancient rocks buried to nearly 8 km. Here, we have accessed new drill core samples which provide an opportunity to understand the dolomitization process in deep basins and its impact on Cambrian carbonate reservoirs. This study documents the origin of the dolostone reservoirs using a combination of petrology, fluid-inclusion microthermometry, and stable and radiogenic-isotopes of outcrop and core samples. An initial microbial dolomitization event (D1) occurred in restricted lagoon environments and is characterized by depleted $\delta^{13}C$ values. Dolomicrite (D2) from lagoonal and sabkha facies, some fabric-retentive dolomite (D3) and fabric-obliterative dolomite (D4) in the peloidal shoal and reef facies show the highest $\delta^{18}O$ values. These dolomites represent relatively early reflux dolomitization. The local occurrence of K-feldspar in D2 indicates some strontium contributed via terrigenous input. Most fabric-retentive dolomite (D3) may have precipitated from seawater at slightly elevated temperatures, suggested by petrological and isotopic data. Most fabric-obliterative dolomite (D4), and medium to coarse dolomite cement (D5), formed between 90 and 130°C from marine evaporitic brine. Saddle dolomite (D6) formed by hydrothermal dolomitization at temperatures up to 170°C, and involved the mixing of connate brines with Sr- enriched hydrothermal fluids. Intercrystalline, moldic, and breccia porosities are due to the early stages of dolomitization. Macroscopic, intergranular, vuggy, fracture, and dissolution porosity are due to buial-related dissolution and regional hydrothermal events. This work has shown that old (e.g. Cambrian or even Precambrian) sucrosic dolomite with associated anhydrite, buried to as much as 8,000 m, can still have a high potential for hosting large hydrocarbon resources and should be globally targeted for future exploration.

Keywords: Carbonate reservoir, dolomitization, hydrothermal fluids, fluid inclusions, C/O/Sr isotopes, restricted lagoon, Cambrian

INTRODUCTION

Dolostone reservoirs represent more than half of all the carbonate rocks globally (Zengler et al., 1980). and offshore China (Zhao et al., 2014) produce significant amounts of petroleum resources. Most of these dolostone reservoirs were initially formed by reflux dolomitizatuon in arid climate environments (Sibley, 1980). Under such circumstances, calcite can be replaced by dolomite by the reflux of evaporated seawater in a restricted platform (Adams and Rhodes, 1960). Refluxing brine could reach underlying porous formations as well as platform margin facies, and induce these strata to be dolomitized under shallow burial conditions (Jiang et al., 2014b; Jones and Xiao, 2005). In addition, a range of other dolomitization processes (such as seawater-, burial- and hydrothermal-dolomitization) can continue through early to burial diagenesis in response to the supply of either locally or externally derived magnesium (Davies and Smith, 2006; Machel, 2004; Smith, 2006).

Deeply buried (3,500 to 8,000 m) Cambrian and Precambrian dolostone reservoirs are currently key exploration targets in both the Sichuan and Tarim Basins of China (Wang et al., 2014; Zhao et al., 2014; Zhu et al., 2015). The Tarim Basin is the largest onshore sedimentary basin in China, with an area of 530,000 km^2 (Fig. 1). The Tarim Basin has suffered multiple phases of tectonic activities (including volcanism) and deformation and dominated by dolostones in the Cambrian and Lower Ordovician Strata. This basin currently produces approximately 6×10^7 m^3 of oil and 9.7×10^9 m^3 of natural gas per year, mostly from Ordovician carbonate reservoirs, which are in part sourced from organic rich Cambrian shales. Exploration for hydrocarbons in potential Cambrian reservoirs in the Tarim Basin is in the early stages.

It has been argued that deeply buried Cambrian dolostones in the Tarim Basin may contain significant hydrocarbon resources (Zhao et al., 2014). This, in addition to localized but widespread source rocks in the lowest Cambrian strata (Cai et al., 2009a; Cai et al., 2009b; Cai et al., 2015b), as well as widespread, thick, regional anhydrite seals (Cai et al., 2015a; Wang et al., 2014) suggests high prospect for future discoveries. Recent exploration has confirmed that large hydrocarbon resources can be found in these very old dolostone reservoirs (Wang et al., 2014). Hydrothermal dolostone in the Upper Cambrian strata of the basin has been recently reported and considered as good reservoirs with porosities of up to 10% even at burial depths of > 8000 m (Dong et al., 2013a; Zhu et al., 2015). The nature and origin of basin-wide, pervasive dolomitization of the Cambrian strata, especially the Lower to Middle Cambrian sections, remains poorly understood.

This paper presents the first comprehensive study of Cambrian dolostone reservoirs across the whole Tarim Basin. The study is based on new data from recently drilled core samples, as well as outcrop samples of Cambrian rocks in the western part of the basin. Conventional core description and wireline logging, transmitted-light petrography, cathodoluminesence (CL) microscopy, and scanning electron microscopy (SEM), fluid inclusion analysis, together with interpretation of C, O and Sr isotopes data, have been utilized to characterize the nature and origin of the dolomitization events that are critical to defining future exploration targets. This dataset has been used to understand the causes of dolomitization events, as well as the role of dolomitization and anhydrite cementation in creating high quality reservoir rocks in the deep Tarim Basin. Specifically, we address the following questions:

1. How many different types of dolomites are present in Cambrian strata in Tarim Basin, and what are their petrological and geochemical characteristics?

2. What mechanisms were responsible for the formation of dolostone reservoirs in the Tarim Basin?

3. What is the role of dolomitization in formation of the good reservoirs in the Tarim Basin?

GEOLOGICAL SETTING

The Tarim Basin is an intracratonic basin surrounded by the Tianshan Mountains to the north, the Kunlun Mountains to the southwest, and the Algyn Mountains to the southeast. The Tarim Basin has been divided into seven tectonic units (Fig. 1).

During the Cambrian, the Tarim plate comprised three isolated carbonate platforms (Western Tarim platform, Western Lop Nor platform, and Kuruktag platform) with relatively deep water sedimentation zones in between (Zhao et al., 2011). Six 3rd-order sequences could be recognized in the Cambrian sections, based on detailed core and outcrop sample observation and facies analyses, and seismic sequence interpretation (Fig. 2) (Liu et al., 2012; Zhao et al., 2011). The most representative and biggest Western Tarim platform was evolved from an isolated platform to a restricted platfrom from the earliest Cambrian to the end of the early Cambrian. During the end of the early Cambrian to the middle Cambrian, this platform dominated by an evaporated platform, and it evolved into a restricted platform again from the end of the middle Cambrian to the late Cambrian (Fig. 3). From bottom to top, the Cambrian strata have been subdivided into six formations (Fig. 2): Yuertusi Formation ($Є_{1y}$), Xiaoerbulake Formation ($Є_{1x}$), Wusonggeer Formation ($Є_{1w}$), Sayilike Formation ($Є_{2s}$), Awatage Formation ($Є_{2a}$), and Qiulitage Formation ($Є_{3q}$) (Fig. 2). $Є_{1y}$ is characteristised by deep basin facies, whereas $Є_{1x}$ is dominated by platform facies and platform margin reef and shoal facies (Fig. 3). Sabkha and other evaporitic sub-environments (e.g. a hypersaline lagoon) are the predominant facies in $Є_{1w}$ and $Є_{2a}$. While $Є_{2s}$ is characterized by platform interior shoal and bank facies (Fig. 3). The uppermost Cambrian strata ($Є_{3q}$) are dominated by restricted carbonate platform facies (Fig. 3).

Several tectonic events led to the formation of 18 unconformities in the Tarim Basin (Fig. 4). The Middle and Upper Ordovician in the eastern Central Tarim and Tabei areas were completely removed as a result of the Caledonian Orogeny (at the end of Ordovician). The Hercynian Orogeny (at the end of Devonian) led to the removal of all the Devonian and/or Silurian strata in most of the Tabei area. The late Yanshannian Orogeny (during the late Cretaceous) resulted in no sedimentation during the Cretaceous in the Southwest Depression. In addition, the Tarim basin experienced four magmatic and/or volcanic activities during the Ediacaran-Cambrian, Early Ordovician, Permian and Cretaceous. Among them the Permian magmactic/volcanic event, which occurred at 290.5 ± 2.9 Ma as constrained by U-Pb isotopic dating (Dong et al., 2013b), was the most intense and had the widest effect on the whole basin.

The burial and geothermal histories of different tectonic units of the Tarim Basin have been previously reported (Qiu et al., 2012; Ye, 1994). The Cambrian strata were quickly buried to a depth ranging from greater than 5,000 m to 8,000 m (Figs. 5A, B, C). The basin was then uplifted by between 2,000 m and 3,500 m before it continued subsiding to reach its current depth. In contrast, the burial history of Keping outcrop area in the northwest Tarim Basin shows that the Cambrian strata were buried to about 4,000 m during the middle Permian. Then the whole section was uplifted to the surface in the early Triassic (Fig. 5D).

METHODS

Approximately 200 core and outcrop samples of Cambrian carbonate (mostly dolostone) were collected from ten recently drilled exploration wells and one outcrop site (Xiaoerbulake) (Fig. 1). Representative samples were selected for detailed petrological (optical transmitted light, cathodoluminescence and scanning electron microscopy), fluid inclusion microthermometry and carbon, oxygen and strontium isotopes. A total of 120 polished thin sections were prepared from dyed, resin-impregnated samples and a small sub-set was stained with alizarin red S (Dickson, 1966) in order to assist with identification of calcite and dolomite. CL observations were made using a Relion III 'cold' cathode device. The operating conditions for the CL microscope were set to 15 kV and 500 μA. Additional observations of the texture and chemistry of phases were made on carbon-coated thin sections using a Philips XL30 scanning electron microscope (back-scattered electron mode) coupled with an energy dispersive X-ray analyser.

Fluid inclusion microthermometic measurements were undertaken on individual dolomite textures using double-polished wafers. Populations of inclusions were carefully characterized (size, distribution, liquid-vapour ratio, presence of hydrocarbons) by transmitted light and UV fluorescence microscopy, and last ice melting (T_m) and homogenization temperatures (T_h) of primary or pseudo-secondary inclusions were measured with a Linkam THMSG 600 fluid inclusion stage. Ice melting temperatures were converted to salinity values (equivalent wt. % NaCl) using standard equations (Bodnar, 2003; Oakes et al., 1990).

Samples of 'bulk' limestone, discrete dolomite crystals and dolomite cements were extracted from clean rock surfaces for carbon ($^{13}C/^{12}C$), oxygen ($^{18}O/^{16}O$) and strontium ($^{87}Sr/^{86}Sr$) isotope analysis using a tungsten-tipped dental burr. Carbon and oxygen isotope ratios were measured in the isotope lab in the School of Environmental Sciences in the University of Liverpool from samples of calcite and dolomite by reacting 4 to 5 mg of powder with 'anhydrous' phosphoric acid at 25°C (~16 h) and 50°C (~48 h) respectively. The product CO_2 was recovered cryogenically and mass ratios were measured using a dual-inlet VG SIRA 10 mass spectrometer. Oxygen isotope ratios were corrected for ^{17}O effects and adjusted for temperature-dependent fractionations associated with the carbonate-phosphoric acid reaction using fractionation factors (α) of 1.01025 for calcite (Friedman and O'Neil, 1977) and 1.01066 for dolomite (Rosenbaum and Sheppard, 1986). Isotopic ratios are reported as delta values with respect to the VPDB carbon and oxygen isotope scales. Analytical precision (1σ) for both calcite and dolomite is better than ±0.1 ‰, based on replicate analysis of in-house quality control materials. Samples for strontium isotope ratio measurement were prepared by dissolving approximately 60mg of powder using ultra-pure acids. Strontium released by acid decomposition was separated by conventional ion exchange techniques and isotope ratios were measured using a Finnigan MAT-262 thermal ionization mass spectrometer at the Institute of Geology and Geophysics, Chinese Academy of Sciences (IGGCAS), Beijing. All $^{87}Sr/^{86}Sr$ values were normalized to a NBS-987 ratio of 0.710253. Analytical precision (2σ) was monitored by repeated measurement of NBS-987 and is better than 0.000015.

RESULTS

PETROGRAPHY

Based on petrographic observations, the diagenetic events including dolomitization, sulphate and calcite cementation, microbial micritization and the creation of caves, mechanical and chemical compaction, neomorphism, petroleum charging, sulphate reduction, and hydrothermal activity have all occurred (Fig. 6). Six dolomite types have been distinguished in the Cambrian strata in the Tarim Basin: microbial dolomudstone (D1), dolomicrite (D2), fabric retentive dolomite (D3), fabric obliterative dolomite (D4), medium to coarse dolomite cements (D5), and saddle dolomite cements (D6). These dolomite types are described in this section.

Microbial dolomudstones (D1)

This type of dolomite consists of very fine crystalline (mostly from 10 to 20 μm crystals), generally planar-e, dark-brown to black, organic-rich laminated dolomudstones (Fig. 6A). They replaced restricted lagoonal and tidal-flat facies. Sedimentary structures including irregular to planar laminations, stromatolites, and bioturbation fabrics, are well preserved in these dolomudstones. There are abundant dolomitized burrows (size from 0.5 to 2 cm) (Baniak et al., 2014) presented in restricted lagoon facies from the top of the Lower ($Є_{1w}$) to the upmost of the Middle ($Є_{2a}$) Cambrian strata. Moreover, microbial rock facies (Zhang et al., 2015) and likely extracellular polymeric substances (EPS) are also presented in the Upper Cambrian stromatolies (You et al., 2013). The above findings suggest that this dolomite type had a microbial origin.

Dolomicrite (D2)

Dolomicrite, locally associated with anhydrite, is predominant dolomite in low energy, restricted facies (e.g. lagoons, sabkhas facies, tidal-flat facies), which is most commonly found in strata from the top of the Lower ($Є_{1w}$) to the Middle ($Є_{2a}$) Cambrian. This dolomite is finely crystalline, with planar-e to planar-s texures (5-20 μm). It consists of light grey, parallel-laminated beds. It is locally associated with dense anhydrite beds and ovoid to irregular anhydrite nodules (from 1 to 10 cm in diameter) (Fig. 6B). This type of dolomite has a dull-red colour under CL (Fig. 6C).

Fabric-retentive dolomite (D3)

Fabric-retentive dolomites are found throughout the whole dolomitized Cambrian section (e.g. $Є_{1x}$, $Є_{2s}$, $Є_{3q}$) and replaced high-energy facies (e.g., oolitic shoal and reef facies) to low-energy facies (e.g. tidal facies). They are composed of fine crystals (10-40 μm) containing a small proportion of finer, planar-e to planar-s dolomite crystals (Fig. 6D). The primary fabrics were composed of peloids, ooids, stromatolites, thrombolites, microbial build-ups, and pebbles. The fabric-retentive, dolomitized oolitic shoals have a very dull-red colour in CL (Fig. 6E).

Fabric-obliterative dolomite (D4)

Fabric-obliterative dolomite consists of medium to coarse-crystalline, planar-s to nonplanar-a dolomite rhombs with a relatively unimodal range of crystal sizes, ranging from 50 to 200 µm. This type is usually present as patches in finer crystalline dolomite (e.g. D3) in the Lower ($Є_{1w}$) to Middle ($Є_{2a}$) Cambrian and as the main lithology type in porous grain/reef dolomites (e.g. $Є_{1w}$, $Є_{2s}$, $Є_{3q}$). The primary fabric has been obliterated by intense recrystallization or replacement of either dolomicrite or primary calcite during progressive burial (Figs. 6F, H). This dolomite shows dull-red to red cathodoluminescence (Figs. 6G, I).

Medium to coarse dolomite cements (D5)

Medium to coarse dolomite cements consist of 50 to 500 µm crystalline, planar-e, and planar-s to nonplanar-a dolomite rhombs with relatively unimodal crystal sizes. In porous dolomite samples, medium to coarse dolomite cement is commonly composed of limpid euhedral crystals (100 to 500 µm) that grew into open pores (Figs. 6D, F, H). This type of dolomite locally fills pores, especially in Upper ($Є_{3q}$), Lower ($Є_{1x}$), and less commonly in Middle ($Є_{2s}$) Cambrian strata. D5 shows red to orange cathodoluminescence (Figs. 6E, G, I).

Saddle dolomite cements (D6)

Saddle dolomite cements consist of coarse-crystalline, nonplanar-a dolomite rhombs with a relatively unimodal crystal size, ranging from 300 µm to 2,000 µm (Fig. 6J). Saddle dolomite has been observed in many fractures and is commonly present at the centre of pores or cavities most commonly in Upper ($Є_{3q}$), and less commonly in Lower ($Є_{1x}$) Cambrian strata. These crystals show typical features of saddle dolomite, such as curved crystal faces and undulose extinction. Saddle dolomite has orange cathodoluminescence (Fig. 6K). The commonly observed saddle dolomite both in this and previous studies, are closely related to deep seated fractures and are probably due to a regional hydrothermal event (Dong et al., 2013b).

Anhydrite beds and cement

Anhydrite is volumetrically significant in the Upper to Middle Cambrian in the reservoir (Figs. 7A, B, Fig. 8G). Anhydrite occurs as beds that are up to 1 metre thick, nodules (from about 500 µm to several centimetres), and as pore-filling cements with a wide range of crystalline sizes and shapes from less than 50 µm to several centimetres (Figs. 7A, B). All of these forms of anhydrite probably originated as gypsum that underwent dehydration during burial. Where abundant, anhydrite locally decreases core plug porosity and permeability. However, porosity is enhanced by fractures in brecciated parts of the Tarim Cambrian and brecciated rocks are most abundant in anhydrite-bearing sections. The timing of formation of breccia is uncertain but it may be linked to early meteoric diagenesis and/or tectonic movements.

Calcite cement

Calcite cement is volumetrically minor throughout the Cambrian strata in the Tarim Basin. Calcite cement is effectively absent in the Lower and Middle Cambrian in the subsurface areas, and there is only a minor occurrence of late-stage fracture-filling calcite mostly in the Upper Cambrian Qiulitage Formation ($Є_{3q}$) (Figs. 7D, E). Where present, calcite cement occurs as coarsely crystalline spar filling in fractures and pore spaces. These petrographically-late forms of calcites have very dull-red or no luminesce (Fig. 6I).

Silica mineral cements

There are two main types of silica mineral cements in the Cambrian of the Tarim Basin. The first type is chalcedony which grows as small (<20 μm) and irregular crystals (Fig. 7B). Chalcedony occurs in association with dolomicrite (D2) and anhydrite nodules, suggesting that it initially formed at relatively low temperature. The second type is vug and fracture filling euhedral quartz cement with crystal size from 50 to >1000 μm (Fig. 7C). This petrographically-late quartz commonly occurs in the Upper Cambrian Qiulitage Formation ($Є_{3q}$) and Middle Cambrian Sayilike Formation ($Є_{2s}$).

Other diagenetic phases

Besides dolomite, calcite, anhydrite, and silica-bearing diagenetic minerals reported above, pyrite, fluorite, barite, and Mississippi Valley Type (MVT) (Davies and Smith, 2006) sulphide minerals are present in the Cambrian strata. Pyrite (FeS_2) is observed across the whole of the Cambrian sections, either replacing the host dolostone or present in the open pore/vug/fracture. MVT deposits locally fill fractures in the Upper Cambrian (Є3q) and contain the following mineral assemblages: galena (PbS), sphalerite (ZnS), pyrite, barite ($BaSO_4$), calcite, dolomite, quartz, and fluorite (CaF_2) (Fig. 7F).

Pore systems in dolostones

Intergranular porosity is predominantly observed in dolomicrite (D2) (Fig. 8A) and fabric retentive dolomite (D3) (Fig. 8B). Macroscopic, intragranular, moldic and dissolution enlarged pores (Fig. 8) are commonly observed in fabric-obliterative dolomite (D4) in the Upper ($Є_{3q}$), Lower ($Є_{1x}$), but are less common in the Middle ($Є_{2s}$) Cambrian strata. Suprastratal fractures pores are abundant in dolomicrite and anhydrite breccias (Fig. 8G) in the Lower ($Є_{1w}$) and Middle ($Є_{2a}$) Cambrian strata. This type of porosity is locally associated with anhydrite dissolution. Fractures have been locally filled by bitumen occurs in Upper ($Є_{3q}$) and Lower ($Є_{1x}$) Cambrian sections (Fig. 8H). Minor amounts of elemental sulphur, sulphide minerals, bitumen, calcite, quartz, fluorite and barite are locally associated with fractures.

Intercrystalline and inter-clast porosity in breccias and anhydrite dissolution pores are most abundant in D2. Point count data show that some D2 samples have porosities ranging between 2% and 10%, but other samples have very low porosity (< 2%) due to pervasive anhydrite cementation. Porosity in D2 represents about three tenths of the overall porosity in the Cambrian units. Moldic and intercrystal porosity in D3 predominantly lies in a range from about 2% to 5%, however, in some cases, porosity in

D3 locally reaches up to 20%. This type of porosity represents about one fifth of the overall porosity in the Cambrian units. Macroscopic intergranular pores are present in fabric-obliterative dolomite (D4) typically from high energy facies (shoal and reef); this type of porosity is commonly greater than 5% and locally up to 12%, and represents about two fifths of the overall porosity in the Cambrian units. Hydrothemal- and fracture-related pores are typically associated with D6. This type of pore is locally present in the Lower ($Є_{1x}$) and Upper ($Є_{3q}$) Cambrian. Fracture-related porosity can represent up to about 10% of a bulk sample but is the least significant type of pore accounting for about one tenth of the overall porosity.Many samples show grain-grain contacts and the occurrence of stylolites suggesting that significant chemical compaction has occurred.

Most of the listed diagenetic events have modified the pore network and thus influenced the reservoir quality of the Cambrian carbonates. However, the focus of this contribution is specifically on dolomitization, which is considered to have played a principal role in controlling the reservoir properties of the investigated rocks. For clarification, we have listed the detailed paragenetic sequence in Figure 9.

FLUID INCLUSION STUDIES

Fluid inclusion assemblages (FIAs) have been defined following the rules of Goldstein and Reynolds (1994) and Goldstein (2012). A consistent FIA is defined as one in which more than 90% of homogenization temperature (Th) data from a given paragenetic type of mineral fall within a range of less than 10-15°C, suggesting it is therefore unlikely that thermal re-equilibration has occurred.

Single phase, aqueous, 1 to 5 μm sized, primary inclusions were found in fabric-retentive dolomite (D3) and small crystalline porphyrotopic dolomite (D5). Host crystals range from 20 to 60 μm in size, and are typically planar-e to planar-s. The presence of single-phase liquid inclusions can be taken to imply that the growth of the host mineral occurred below about 50°C (Goldstein and Reynolds, 1994).

Two-phase, liquid-gas, primary fluid inclusions were found in coarsely crystalline, fabric-obliterative dolomite (D4), medium to coarse dolomite cements (D5), and saddle dolomite cements (D6). These varied in size from about 3 μm to 15 μm. Measured homogenization temperatures fall predominantly between 90°C and 170°C for saddle dolomite, whereas fabric obliterative-dolomite (D4) and medium to coarse dolomite cements (D5) show a relatively lower and narrow temperature range from 90°C to 130°C (Fig. 10A).

Salinity data from the fluid inclusions, derived from observed measurements of the last ice melting temperatures, indicate that water present at the time of growth of fabric-obliterative dolomite (D4) and medium to coarse dolomite cements (D5) ranged from 6 wt % to 14 wt %, although a few samples reached 20 wt % (Fig. 10B). In contrast, saddle dolomite (D6) samples precipitated from more saline waters (10 wt % to 26 wt %), with salinity being greater than 18 wt % in most cases (Fig. 10B). Overall, there is no simple relationship between salinity and temperature during dolomite growth (Fig. 11). However, fabric-obliterative dolomite (D4) and medium to coarse dolomite (D5) cements grew at relatively lower temperature and salinity, whereas saddle dolomite (D6) precipitated at rather higher temperature and salinity but over a relatively wide range of values (Fig. 11).

ISOTOPE DATA

Stable isotopes

The results of stable isotope (O and C) analyses are presented in Figure 8 and Table 1. Five limestone samples (micrite) display a relatively narrow isotopic range, lying between -2.06 and 0.01 ‰ VPDB for $\delta^{13}C$, and between -7.30 and -5.9 20 ‰ VPDB for $\delta^{18}O$. Microbial dolomudstone (D1) samples show relatively negative $\delta^{13}C$ values ranging from -6.46 to -2.46 ‰, and a narrow range of $\delta^{18}O$ values between -6.00 and -5.35 ‰ (Fig. 12). Dolomicrite (D2) samples show a $\delta^{13}C$ range from -0.87 to 1.32 ‰, and a narrow $\delta^{18}O$ range between -6.70 and -5.35 ‰ (Fig. 12). Previously reported dolomicrite (D2) yielded a higher maximum $\delta^{18}O$ value of up to -3.00 ‰ (Zheng et al., 2013). $\delta^{13}C$ and $\delta^{18}O$ values for the fabric-retentive dolomite (D3) are similar to those of the limestone samples ($\delta^{13}C$ from -2.79 to -0.18 ‰; $\delta^{18}O$ from -7.38 to -6.17 ‰; Fig. 12). Fabric-obliterative dolomite (D4) samples have $\delta^{13}C$ values between -1.71 and 2.89 ‰ and $\delta^{18}O$ values between -8.01 and -5.63 ‰ (Fig. 12). Samples taken from medium to coarsely crystalline dolomite cement (D5) have a narrow $\delta^{13}C$ and $\delta^{18}O$ range (-2.27 to 0.19 ‰ and -8.93 to -7.70 ‰ respectively) (Fig. 12). Coarsely crystalline saddle dolomite isotope data (D6) represent a distinct group that is typified by largely negative $\delta^{13}C$ values (-4.33 to 0.14 ‰) and the lowest $\delta^{18}O$ values (-11.83 to -9.06 ‰) (Fig. 12).

Strontium isotope

Four limestone samples yielded a narrow range of $^{87}Sr/^{86}Sr$ from 0.7088 to 0.7094 (Fig. 13). The dolomicrite (D2), fabric-retentive dolomite (D3), fabric-obliterative dolomite (D4) and medium to coarse dolomite cement (D5) have narrow, broadly similar ranges of $^{87}Sr/^{86}Sr$ from 0.7087 to 0.7093, except one dolomicite sample that has a relatively high $^{87}Sr/^{86}Sr$ value of 0.710794 (Fig. 13). However, saddle dolomite cements (D6) have higher $^{87}Sr/^{86}Sr$ values, falling between 0.7093 and 0.7010 (Fig. 13).

DISCUSSION

DOLOMITE PARAGENESIS

Dolomite crystals in microbial dolomudstones (D1) and dolomicrite (D2), from the restricted and tidal-flat facies, are generally euhedral and have the smallest crystal size (5-20 μm). These two types commonly represent the initial phase of dolomitization in sedimentary basins (Haas et al., 2014; Machel, 2004); D1 and D2 grew at the very early stage of burial diagenesis at depths <500 m (Al-Helal et al., 2012; Jiang et al., 2014b). Fabric-retentive dolomite (D3) also has a relatively small dolomite crystal size (10-40 μm) but preserved the original grain fabrics. Hence D3 also represents a relatively early stage of dolomitization during shallow burial environments (e.g. < 1,000 m) (Ehrenberg et al., 2006) but after D1 and D2. Thus D3 probably grew at between 500 m and 1,000 m burial.

Fabric-obliterative dolomite (D4) and medium to coarse dolomite cements (D5) commonly have larger crystal size (50-500 μm) and are planar-s to nonplanar-a. These characteristics are consistent with burial dolomite which probably formed during medium to deep burial (e.g. ~1000 to 3500 m) (Ehrenberg et al., 2006; Machel, 2004), although some research has found that fabric-obliterative dolomite may also be formed at relatively shallow burial, probably during early diagenesis (e.g. < 700 m) associated with fabric-retentive dolomite (Martín-Martín et al., 2015). D5 commonly grew in pores and on top of D4, suggesting that D5 precipitated after D4 (Figs. 4H, I). Saddle dolomite cements (D6) typically grew in vugs and fractures. The limpid, nonplanar-a D5 is locally cut or overlain by D6 in fractures and vugs, suggesting that D6 precipitated later than D5.

CAUSES OF DOLOMITIZATION IN THE CAMBRIAN CARBONATES

The key attributes of the various types of dolostone in the Cambrian strata in the Tarim Basin are summarized in Table 2 and Figure 14. There are clear differences in the microbial dolomudstone (D1), dolomicrite (D2), fabric-retentive dolomite (D3), fabric-obliterative dolomite (D4), and dolomite cements (D5 and D6), in terms of crystal shape and size, isotopes, and fluid-inclusion temperatures and salinities. The nature of multistage dolomitization in the Cambrian carbonates in the Tarim Basin can be reconstructed by integrating information on the spatial distribution of sedimentary facies, with the diagenetic paragenesis and geochemical results presented above, taking into account the available regional geological and burial history data (Fig. 14, Table 2). The characteristics of the vast majority of the Cambrian dolomite, locally interbedded with rare laminated limestone, supports models of pervasive fluid throughput and dolomitization (Machel, 2004). In the following sections, we discuss the plausibility of various models for dolomitization.

Evaluation of the role of microbial dolomitization

Available well data are consistent with large areas of restricted lagoon facies being present in the upper part of the Lower ($Є_{1w}$) and Middle ($Є_{2a}$) Cambrian strata in the Tarim Basin (Zheng et al., 2013). Extracellular polymeric substances (EPS) and dolomitized burrows have been found in these microbial dolomudstone (D1) (You et al., 2013). These dolomite in D1 rocks are characterized by depleted $\delta^{13}C$ values (down to less than -6 ‰; Fig. 12). Using the dolomite-water oxygen-isotope fractionation equation of Vasconcelos et al. (2005) for low-temperature dolomitization, and assuming a temperature of 20 to 25°C for the surface temperature conditions (You et al., 2013), the $\delta^{18}O$ of the water present during the growth of D1 was between -7.33 and -5.23 ‰ VSMOW (Fig. 15). Employing the Friedman and O'Neil (1977) calcite-water oxygen-isotope fractionation equation and the assumption that the micrite oxygen isotope values were not altered by subsequent burial and diagenesis, the $\delta^{18}O$ of Cambrian seawater in the study area is interpreted to be in the range from -8.88 to -4.71 ‰ VSMOW. The broad overlap of the calculated water oxygen isotope values of D1 with micrite suggests that normal seawater (salinity at ~3.5 wt %) was the predominant dolomitization fluid for D1.

In modern environments, bacterial sulphate reduction (BSR) can play an important role in the precipitation of dolomite at near-surface temperatures (Vasconcelos et al., 1995; Warthmann et al., 2000). Such phenomena have been observed in hypersaline lagoons of Lagoa Vermelha and Brejo do Espinho, northeastern coast of Brazil (Vasconcelos et al., 2005; Warthmann et al., 2000), ephemeral lakes of the Coorong Region of South Australia (Wright and Wacey, 2005) and sabkha environments in Abu Dhabi (Bontognali et al., 2010). However, based on detailed cation ordering comparison, Gregg et al (2005) recently argued that very high-Mg calcite (VHMC) rather than dolomite as claimed previously (Vasconcelos et al., 1995; Warthmann et al., 2000) was synthesized under ambient conditions by means of microbial catalysis. Microbial mats, EPS, and animal burrows can serve as templates to facilitate dolomitization (Baniak et al., 2014; Machel et al., 2014). It is likely that microbially-mediated VHMC initially grew in the Cambrian strata in the Tarim Basin at ambient conditions, and VHMC may have transformed into ordered dolomite through a dissolution-re-precipitation reaction during diagenesis (Gregg et al., 2015).

Sabkha and reflux dolomitization

The upper part of the Lower ($Є_{1w}$) and Middle Cambrian ($Є_{2a}$) sections in the Tarim Basin are characterized by carbonates interbedded with anhydrite-dominated evaporites. The formation of dolomicrite (D2) by evaporitic brine is supported by relatively heavy $\delta^{18}O$ values, from -5 to -6.5‰ (and higher published values $\delta^{18}O$ values; Fig. 12). Using the dolomite-water oxygen-isotope fractionation equation (Vasconcelos et al., 2005) for low-temperature dolomitization, and assuming temperatures of 30°C to 35°C, i.e. slightly greater than surface during an arid climate, then the $\delta^{18}O$ of the water present during the growth of dolomicrite (D2) was between -5.78 and -1.21 ‰ VSMOW (Fig. 15). Published global values for $\delta^{18}O$ in brachiopods in Cambrian strata are in the range from -10 to -7 ‰ VPDB (Veizer et al., 1999) similar to the values determined for the coeval micrite (mainly -7.5 to -7 ‰ with one exception at about -6 ‰; Fig. 12). These data are consistent with evaporation resulting in a 3.5 ‰ increase of oxygen isotope ratios of the evaporated Cambrian seawater (from -8.88 to -4.71 ‰ VSMOW).

Moreover, abundant early diagenetic gypsum (now transformed to anhydrite) occurs in association with dolomicrite (D2) in the Lower ($Є_{1w}$) and Middle Cambrian ($Є_{2a}$) (Figs. 2 and 3). This supports models of sabkha capillary zone dolomitization (Kinsman, 1966; Machel, 2004) and reflux dolomitization (Adams and Rhodes, 1960) being appropriate for the formation of D2 in the Tarim Basin. Therefore the salinity of the dolomitizing water for D2 was probably close to gypsum saturation. In such circumstance, evaporation of seawater increases the Mg:Ca ratio thus promoting dolomite precipitation. Dolomitization then decreases the Mg:Ca ratio and increases the Ca^{2+} concentration which, in turn, promotes gypsum formation. Growth of gypsum subsequently results in an increase in the Mg:Ca ratio. Hence, coeval dolomitization and gypsum precipitation in sabkha and restricted lagoon settings are sustainable as long as there is periodic input of new seawater. Interestingly, some fabric-retentive dolomite (D3) and fabric-obliterative dolomite (D4), from the reef and shoal facies, have overlapping $\delta^{18}O$ values with dolomicrite (Fig. 12). ^{18}O enriched evaporitic water (from -5.78 to -1.21 ‰ VSMOW) may also have been responsible for the formation of isotopically-enriched D3 and D4. This seems to be reasonable because refluxing brine could percolate into the underlying porous carbonates deposited in high-energy facies (e.g. reef and shoal facies), and result in these carbonates being dolomitized (Al-Helal et al., 2012; Jiang et al., 2013; Jones and Xiao, 2005).

$\delta^{13}C$ values of limestone samples, and most of the D2, D3, and D4 samples (Fig. 12), all lie within the reported range of Cambrian seawater $\delta^{13}C$ values ($\delta^{13}C$ -2.5 to 2 ‰) (Montañez et al., 2000; Veizer et al., 1999). Furthermore, the $^{87}Sr/^{86}Sr$ values of limestones, D2, D3, and D4 all lie in a narrow range from 0.7080 to 0.7094, typical of Cambrian seawater $^{87}Sr/^{86}Sr$ values (Montañez et al., 1996; Montañez et al., 2000; Veizer et al., 1999). Therefore, the isotopic geochemistry of $\delta^{13}C$ and $^{87}Sr/^{86}Sr$ supports the dolomitization fluids for D2, some D3 and D4, being caused by the evaporation of Cambrian seawater. However, one dolomicrite (D2) sample has an anomalously high $^{87}Sr/^{86}Sr$ value of 0.710794 (Table 1; Fig. 13). This sample is locally enriched in K-feldspar (observed in the SEM). Thus, D2 samples with $^{87}Sr/^{86}Sr$ values higher than that of coeval seawater may have incorporated some radiogenic ^{87}Sr resulting from the breakdown of radioactive ^{87}Rb, noting that Rb can easily substitute for potassium in K-feldspar.

Shallow-burial seawater dolomitization

The $^{87}Sr/^{86}Sr$ (Fig. 13) and $\delta^{13}C$ (Fig. 8) values for some fabric-retentive dolomite samples (D3) samples are similar to Cambrian seawater, consistent with seawater being the predominant dolomitization fluid. D3 dolomite samples have relatively high oxygen isotope values (-7.5 to -6.5 ‰ VPDB; Fig. 12). Assuming that the formation temperature of these D3 samples was about 40°C (i.e. only slightly higher temperature than that assumed for dolomicrite, D2), and employing the same dolomite-water oxygen-isotope fractionation equation (Vasconcelos et al., 2005), then the calculated water present during the growth of D3 was between -4.94 and -3.91 ‰ VSMOW (Fig. 15). Similarly, employing the Friedman and O'Neil (1977) calcite-water oxygen-isotope fractionation equation, the $\delta^{18}O$ of Cambrian seawater in the study area was in the range from -4.88 to -1.78 ‰ VSMOW at the same temperature. The general overlap of the above calculations leads us to conclude that seawater may have been the principal dolomitizing fluid during the early burial stage (most likely < 500 m, assuming the surface temperature of 25°C, and a normal geothermal gradient value of 30°C/km).

Seawater dolomitization was a recent addition to the array of dolomitization models; it has been reported to occur over a wide range of depths from shallow burial to intermediate burial, where circulation of seawater induced by thermal convection is considered to be responsible for the formation of massive dolostones (Machel, 2004; Whitaker and Xiao, 2010). Fabric-retentive dolomite samples (D3) are predominantly found in the top part of the Middle Cambrian through to Upper Cambrian units from the platform margin areas (Fig. 1; Table 1). This matches well previously published reactive transport modelling output showing that a dolomite body generated by geothermal convection was initially restricted to a narrow zone at the platform margin, although large parts of the platform could be completely dolomitized over a relatively prolonged period, e.g. 30 m.y. (Whitaker and Xiao, 2010). Shallow-buried seawater dolomitization played an important role in the formation of massive dolostone bodies in the Upper Permian to Lower Triassic dolostone reservoirs in the Sichuan Basin, China (Jiang et al., 2014b). Studies of the partial to complete dolomitization of shallow-marine Cenozoic carbonates, at a depth range from tens to hundreds of metres in the Bahamas and Cayman Islands, demonstrated that shallow-burial (mostly < 1000 m) dolomitization with normal seawater is dominant in isolated carbonate platforms (Budd, 1997; Jones et al., 2003; Melim et al., 2001). In the seawater-dolomitization model, early dolomite might act as a nucleus for later, more pervasive dolomitization during shallow burial diagenetic environments (Machel, 2004).

Medium to deep-burial dolomitization

The burial history of Cambrian strata derived from three different wells and one outcrop represent different regions across the Tarim Basin (Fig. 5), and are consistent with a continuous and rapid subsidence after deposition. As a result, Cambrian carbonates reached a depth of about 4,500 m to > 6,000 m during the early Ordovician across most of the Tarim Basin. The highest temperatures that the Cambrian strata reached were from 180 to 240°C (Fig. 5). Hence, burial dolomitization likely has been favoured at such elevated temperature conditions, either by replacement of remaining calcite during intermediate burial settings (Machel, 2004), by recrystallization of the earlier formed dolomite (Jiang et al., 2014b), or by fracture-filling, medium to coarsely crystalline dolomite cements (Gomez-Rivas et al., 2014; Haas et al., 2014).

The similarities of the $\delta^{13}C$, $\delta^{18}O$ and $^{87}Sr/^{86}Sr$ isotopes between some fabric-obliterative dolomite (D4) samples and all medium to coarse dolomite cement (D5) samples (Figs. 12 and 13), suggest that D4 and D5 dolomites may have precipitated from similar fluids. The $\delta^{13}C$ and $^{87}Sr/^{86}Sr$ isotope values are comparable to the early dolomites (D2, D3) and remaining limestones (Figs. 12 and 13), possibly suggesting that Cambrian seawater was the predominant agent of dolomitization for D4 and D5 as well. However, the depleted oxygen isotope values ($\delta^{18}O$ -9.0 to -7.5 ‰ VPDB) of D4 and D5, and the relatively higher growth temperatures (90 to 130°C for D4 and D5; Fig. 10A), confirm that D4 and D5 formed in burial environments at a depth range from about 2000 to 3000 m (Fig. 5). Using the relevant fluid inclusion temperature data of 90 to 130°C and dolomite-water oxygen-isotope fractionation equation for high temperature dolomite (Land, 1983), the calculated $\delta^{18}O$ value of the dolomitization water for D4 and D5 falls in a range between 2.20 to 5.23 ‰ VSMOW (Fig. 15). These values are slightly depleted relative to the calculated water isotopes derived from seawater (5.50 to 6.38‰ VSMOW) using the Friedman and O'Neil (1977) calcite-water oxygen-isotope fractionation equation within the same temperatures. This seems to suggest the incorporation of isotopically lighter water, such as meteoric water or connate seawater and brines.

Salinity data from aqueous inclusions in D4 and D5 show that this burial stage dolomitization water had relatively high salinity (6 to 20 wt %) (Fig. 10A), precluding the possibility of meteoric water influx. During deep burial environments, water associated with anhydrite dissolution and TSR-generated water commonly have relatively depleted $\delta^{18}O_{VSMOW}$ value compared to the evolved connate formation water (Jiang et al., 2015a; Jiang et al., 2015c; Worden et al., 1996). Abundant anhydrite in the presence of petroleum, H_2S concentrations up to 11% (Cai et al., 2015b; Cai et al., 2016; Worden and Smalley, 1996), and temperatures > 110°C all show that TSR has occurred in the Lower to Middle Cambrian dolostones. Hence, the negative shift of the water $\delta^{18}O$ value possibly indicates the incorporation of TSR water or connate saline brine from the Lower to Middle Cambrian anhydrite enriched strata (e.g. $Є_{1w}$, $Є_{2a}$).

Hydrothermal dolomitization

Saddle dolomite cements (D6) in the Lower ($Є_{1x}$) and Upper ($Є_{3q}$) Cambrian show depleted oxygen isotope values ($\delta^{18}O$: -12 to -9 ‰ VPDB), discrete from D4 and D5 values, and have the highest precipitation temperatures (with aqueous fluid inclusion homogenization temperatures from 90 to 170°C; Fig. 10). Moreover, D4 and D5 dolomites types are locally overgrown by D6 in open pores. Hence, D6 formed after D4 and D5 and precipitated at an elevated temperature. Relatively high salinities from D6 fluid inclusions (from 10 to 26 wt % NaCl; Fig. 10A), show that the D6 dolomitization fluid was more saline than that responsible for the precipitation of D4 and D5. Moreover, the elevated $^{87}Sr/^{86}Sr$ ratios of D6 are higher than the $^{87}Sr/^{86}Sr$ values of Cambrian seawater (Fig. 13). This, together with the highest diagenetic temperatures, suggests that there were episodes of invasion of the deeper and hotter basinal fluids that leached Sr from potassium-bearing rocks (e.g. clastic sediments with K-feldspar or mica minerals) during the growth of D6. Therefore, saddle dolomite (D6) in this study is probably hydrothermal, and comparable to reported hydrothermal dolomite occurrences (HTD) worldwide (Davies and Smith, 2006).

Stable carbon isotope values from saddle dolomite (D6) are similar to most of the other types of dolomites, as well as to that of the marine precipitates (Fig. 12), suggesting that the parent fluid inherited the original seawater carbon signal (i.e. it was a rock-buffered system). Using the dolomite-water oxygen-isotope fractionation equation of Land (1983) for high temperature dolomite, the calculated water $\delta^{18}O$ responsible for D6 lies in a range between 3.43 to 7.27 ‰ VSMOW over the fluid inclusion-defined temperature range (90 to 170°C) (Fig. 15). This is lower than the calculated water oxygen isotopes derived from seawater (5.50 to 9.34 ‰ VSMOW). Hence, the involvement of more saline brine and possibly TSR-derived water in D6 seems likely (as discussed above).

Base metal minerals (e.g. barite, galena, and sphalerite) (Fig. 7F) and saddle dolomite (D6) are locally present in fractures showing similar petrological and geochemical characteristics to previously reported saddle dolomite in Upper Cambrian and Ordovician strata (Dong et al., 2013a; Jiang et al., 2015b). The growth of hydrothermal dolomite was controlled by the fault and fracture in outcrop samples and has been proved to be closely related to the Permian hydrothermal event with an age of 290.5 ± 2.9 Ma constrained by U-Pb isotopic dating (Dong et al., 2013b). Hence, the invasion of hydrothermal fluids along basement-rooted fractures and faults was most likely responsible for the precipitation of D6 in this study. An effective method to evaluate whether dolomite is of hydrothermal origin, is to determine when the dolomitization occurred and then compare the burial temperature to fluid inclusion homogenization temperature in dolomites (Davies and Smith, 2006; Smith, 2006). According to the burial histories from different wells in different areas of Tarim Basin, the maximum palaeo-temperatures are 100 to 180°C for the Cambrian and 60 to 140°C for the Ordovician (Fig. 5). In contrast, in the outcrop area, both Cambrian and Ordovician strata were never buried deep enough for the normal conduction-controlled temperature to exceed 160°C (Fig. 5) although growth occurred at >160°C, as evidenced from fluid inclusions (Fig. 10). Hence, these saddle dolomites can be unequivocally called hydrothermal (Machel and Lonnee, 2002). The temperature of saddle dolomite in the Cambrian strata from the subsurface area is equal to, or less than, the maximum burial temperature. However, similar geochemical features and homogenization temperatures for both outcrop and subsurface saddle dolomite indicate that they may have precipitated from similar fluid during the same period. Thus, all the saddle dolomite samples in this study may have been formed during early to medium burial and/or uplift stages when burial temperatures were relatively low (e.g. <100°C) (Smith, 2006).

THE IMPACT OF DOLOMITIZATION ON RESERVOIR QUALITY IN DEEPLY BURIED CARBONATE

Porous dolostone reservoirs

According to a systematic statistical evaluation with data collected from many carbonate platform successions worldwide, porosity and permeability vary as a function of burial depth (Ehrenberg et al., 2006; Sun, 1995). Specifically, porosity of relatively shallow-buried (< 3500m), younger dolostones (e.g. Pliocene-Pleistocene and Miocene dolostone and Miocene dolostone) is typically equal to, or less than, the porosity of their age-equivalent limestone. However there are some exceptional dolostone reservoirs that have higher porosity than their limestone counterparts when the dolomite formed due to shallow-burial processes (e.g. the First Eocene reservoir at the giant Wafra Field, Saller et al., 2014; the Miocene carbonate platforms of the Marion Plateau, Ehrenberg et al., 2006). When the burial depth becomes greater than 3,500m and up to a maximum of about 8,000m, however, dolostone tends to have better reservoir quality than their limestone counterparts (Cai et al., 2014; Ehrenberg et al., 2006; Heydari, 1997; Jiang et al., 2014b; Sun, 1995). This is because dolostone is more resistant than limestone to the porosity-reducing effects of burial (i.e., mechanical and chemical compaction and cementation) (Schmoker and Halley, 1982), and dolostone is more likely to possess open and effective fracture systems at deep burial (> 3500 m) than limestones (Hugman III and Friedman, 1979).

The amount of porosity found in deeply buried (> 3,500 m) dolostone reservoirs is usually considered to be a complex function of the primary porosity, the amount of secondary porosity due to the mole-for-mole replacement or dissolution of the calcite or aragonite by dolomite, and the degree of preservation of the early diagenetic porosity (Ehrenberg et al., 2006; Ehrenberg et al., 2012; Machel, 2004; Sun, 1995). Some have recently argued that significant porosity could be newly formed or pre-existing porosity redistributed due to the dissolution of dolomite and anhydrite in deeply buried dolostone reservoirs due to thermochemical sulphate reduction (TSR) (Cai et al., 2014), as well as due to hydrothermal dolomitization, fluids mixing and cooling, fracture system formation and brecciation (Corbella et al., 2004; Davies and Smith, 2006; Gomez-Rivas et al., 2014; Hiemstra and Goldstein, 2015; Jiang et al., 2015b; Machel, 2004; Martín-Martín et al., 2015; Qing and Mountjoy, 1994; Saller and Dickson, 2011; Smith, 2006; Sun, 1995). It is likely that more than one of the above diagenetic processes has affected reservoir quality in the Cambrian reservoirs in the Tarim Basin.

The origin of porosity in the Cambrian dolostones and future exploration targets in the Tarim Basin

Moldic pores and intercrystalline porosities are commonly observed in the shoal and reef facies in both fabric-retentive dolomite (D3) and fabric-obliterative dolomite (D4) in the Lower (Є$_{1x}$) and Middle (Є$_{2s}$) Cambrian sections. Point count data show that moldic porosity mainly lies in a range from about 2% to 5%, and represents of about 20% of the overall porosity in the Cambrian units. These types of porosity (intercrystalline, moldic and breccias) were probably generated by a relatively early stage of hypersaline dolomitization in an arid climate (Jiang et al., 2014a; Machel, 2004; Saller et al., 2014; Sun, 1995). Macroscopic intergranular pores are commonly present in fabric-obliterative dolomite (D4) in high energy, grain shoal and reef facies in the Lower (Є$_{1x}$) and Middle (Є$_{2s}$) Cambrian sections are predominantly due to the preservation of the primary porosity (Sun, 1995) and subsequent dissolution (e.g. bacterial sulphate reduction or thermochemical sulphate reduction) (Cai et al., 2014; Saller et al., 2014). This dolostone type has porosity commonly greater than 5% and locally up to 12%. Hydrothermal- and fracture-related, vuggy and late diagenetic dissolution pores are presumably related to the burial corrosion (e.g. BSR and TSR) and hydrothermal events. The corrosion fabrics are commonly observed in the platform facies in the Upper Cambrian strata and are probably related to the regional hydrothermal activity (Davies and Smith, 2006; Dong et al., 2013a; Hiemstra and Goldstein, 2015; Jiang et al., 2015b; Saller and Dickson, 2011).

Overall, early dolomitization (D2 and D3) was fundamental in forming intercrystalline and modic porosities. Early anhydrite precipitation in D2 locally reduced porosity to negligible values where it is present. However, early fracturing and brecciation provided an opportunity for sulphate reduction during later burial. These diagenetic events have significantly enhanced porosity in D2. Mesogenetic dissolution occurred during further burial, resulting in the volumetrically significant macroscopic intergranular porosity in D4, and vuggy and fracture porosity in D6. Thermochemical sulphate reduction and hydrothermal fluids were probably responsible for the macroscopic dissolution in these deeply burial environments. The regional thick anhydrite layers performed as a good seal for the underlying sucrosic dolostone reservoirs from high energy facies in the Lower (Є$_{1x}$) and Middle (Є$_{2s}$) Cambrian sections, as well as for the anhydrite bearing dolomicrite reservoir from restricted facies in the top of the Lower (Є$_{1w}$) to Middle (Є$_{2a}$) Cambrian sections. The widespread lowermost Cambrian basinal mudstone and shales are considered to be the main petroleum source rock for the Cambrian reservoirs. Upper Cambrian strata (Є$_{3q}$) also have relatively high porosities (locally up to >10 %) (Fig. 2). However, due to the absence of regional seals, these Upper Cambrian dolostone reservoirs are unlikely to host significant amounts of hydrocarbons. Hence, this study has shown that the main exploration targets in the deeply-buried Cambrian strata in the Tarim Basin are sucrosic dolostone reservoirs (D3, D4) in the Lower (Є$_{1x}$) and Middle (Є$_{2s}$) Cambrian sections, as well as anhydrite-enriched dolomicrite reservoirs (D2) in the Lower (Є$_{1w}$) and Middle (Є$_{2a}$) Cambrian sections. This study further shows that other sedimentary basins that have similar geological settings and lithology associations (dolomites and anhydrites) as the Tarim Basin, probably have porous dolostone reservoirs, despite the very deep buried, which may host significant petroleum resources for exploration in future.

CONCLUSIONS

(1) This study has provided a comprehensive analysis of the nature and evolution of dolomitic Cambrian reservoirs. Six distinct dolomite types and five dolomitization events have been characterized in terms of their fabrics, paragenetic sequences, isotopic characteristics, and fluid inclusions.

(2) The presence of burrows and EPS in the low energy facies (e.g. restricted lagoon) and the depleted $\delta^{13}C$ values suggest that the microbial mediated dolomitization (D1) probably occurred; this represents the initial dolostone phase.

(3) Dolomicrite (D2) is commonly associated with anhydrite in the lagoonal and sabkha facies and represents the second, relatively early, dolomitization phase. This was caused by sabkha and reflux dolomitization at a temperature ranging from 30 to 35°C. Some fabric-retentive dolomite (D3) and fabric-obliterative dolomite (D4) in the peloidal shoal and reef facies were probably created by the same brine reflux.

(4) Seawater dolomitization, supported by $^{87}Sr/^{86}Sr$, $\delta^{13}C$ values and water oxygen isotope ratio calculation was most likely responsible for some diagenetic fabric-retentive dolomite (D3) at the temperature of about 40°C.

(5) Some fabric-obliterative dolomite (D4) and medium to coarse dolomite cement (D5) were formed during medium to deep-burial (1000-3500 m) environments, at temperatures range between 90 and 130°C, and involved mixing of water derived from marine evaporites from the Middle Cambrian strata with the connate seawater.

(6) Saddle dolomite (D6) represents the last stage dolomitization, which was due to hydrothermal dolomitization at temperatures ranging from 90 to 170°C. D6 records an influx of the connate Cambrian brines and base metal-enriched hydrothermal fluids, resulting in the elevated salinity and strontium-isotope values.

(7) Early dolomitization (D2 and D3) was fundamental in forming intercrystalline and moldic porosities. Early fracturing and brecciation provided an opportunity for later sulphate reduction during burial; together these diagenetic events significantly enhanced porosity in D2. Mesogenetic dissolution caused by thermochemical sulphate reduction and hydrothermal fluids, was also responsible for the generation of volumetrically significant macroscopic intergranular porosity in D4, and vuggy and fracture porosity in D6.

(8) This study suggests that deeply buried (up to >8,000 m), sucrosic dolostone reservoirs from the Lower to Middle Cambrian sections, anhydrite-enriched dolomicrite reservoirs have good porosities.

Other similar deeply buried sedimentary basins worldwide should be considered prospective for petroleum exploration.

ACKNOWLEDGMENTS:

This work has been financially supported by China National Funds for Distinguished Young Scientists (41125009), Special Major Project on Petroleum Study (2016ZX05008003-040), the Natural Science Foundation of China (41402132) and a scholarship under the International Postdoctoral Exchange Fellowship Program (20150035) supported by the Office of China Postdoctoral Council (OCPC).

REFERENCES

Adams, J.E. and Rhodes, M.L. (1960) Dolomitization by seepage refluxion. *American Association of Petroleum Geologists, Bulletin*, **44,** 1912-1920.

Al-Helal, A.B., Whitaker, F.F. and Xiao, Y. (2012) Reactive transport modeling of brine reflux: dolomitization, anhydrite precipitation, and porosity evolution. *Journal of Sedimentary Research*, **82,** 196-215.

Baniak, G.M., Amskold, L., Konhauser, K.O., Muehlenbachs, K., Pemberton, S.G. and Gingras, M.K. (2014) Sabkha and Burrow-Mediated Dolomitization in the Mississippian Debolt Formation, Northwestern Alberta, Canada. *Ichnos*, **21,** 158-174.

Bodnar, R.J. (2003) Reequilibration of fluid inclusions. In: *Fluid Inclusions—Analysis and Interpretation; Special Publication* (Eds I. Sampson, A. Anderson and D. Marshall), **32**, pp. 213-231. Mineralogical Association of Canada.

Bontognali, T.R., Vasconcelos, C., Warthmann, R.J., Bernasconi, S.M., Dupraz, C., Strohmenger, C.J. and McKenzie, J.A. (2010) Dolomite formation within microbial mats in the coastal sabkha of Abu Dhabi (United Arab Emirates). *Sedimentology*, **57,** 824-844.

Budd, D.A. (1997) Cenozoic dolomites of carbonate islands: their attributes and origin. *Earth-Science Reviews*, **42,** 1-47.

Cai, C.F., Amrani, A., Worden, R.H., Xiao, Q.L., Wang, T.K., Gvirtzman, Z., Li, H.X., Said-Ahmad, W. and Jia, L.Q. (2016) Sulfur isotopic compositions of individual organosulfur compounds and their genetic links in the Lower Paleozoic petroleum pools of the Tarim Basin, NW China. *Geochimica et Cosmochimica Acta*, **182**, 88–108.

Cai, C.F., He, W.X., Jiang, L., Li, K.k., Xiang, L. and Jia, L.q. (2014) Petrological and geochemical constraints on porosity difference between Lower Triassic sour-and sweet-gas carbonate reservoirs in the Sichuan Basin. *Marine and Petroleum Geology*, **56,** 34-50.

Cai, C.F., Hu, G.Y., Li, H.X., Jiang, L., He, W.X., Zhang, B.S., Jia, L.Q. and Wang, T.K. (2015a) Origins and fates of H_2S in the Cambrian and Ordovician in Tazhong area: Evidence from sulfur isotopes, fluid inclusions and production data. *Marine and Petroleum Geology*, **67,** 408-418.

Cai, C.F., Li, K.K., Ma, A.L., Zhang, C.M., Xu, Z.M., Worden, R.H., Wu, G.H., Zhang, B.S. and Chen, L.X. (2009a) Distinguishing Cambrian from Upper Ordovician source rocks: Evidence from sulfur isotopes and biomarkers in the Tarim Basin. *Organic Geochemistry*, **40,** 755-768.

Cai, C.F., Zhang, C.M., Cai, L.L., Wu, G.H., Jiang, L., Xu, Z.M., Li, K.k., Ma, A.L. and Chen, L.X. (2009b) Origins of Palaeozoic oils in the Tarim Basin: Evidence from sulfur isotopes and biomarkers. *Chemical geology*, **268,** 197-210.

Cai, C.F., Zhang, C.M., Worden, R.H., Wang, T.K., Li, H.X., Jiang, L., Huang, S.Y. and Zhang, B.S. (2015b) Application of sulfur and carbon isotopes to oil–source rock correlation: A case study from the Tazhong area, Tarim Basin, China. *Organic Geochemistry*, **83,** 140-152.

Corbella, M., Ayora, C. and Cardellach, E. (2004) Hydrothermal mixing, carbonate dissolution and sulfide precipitation in Mississippi Valley-type deposits. *Mineralium Deposita*, **39,** 344-357.

Davies, G.R. and Smith, L.B. (2006) Structurally controlled hydrothermal dolomite reservoir facies: An overview. *American Association of Petroleum Geologists, Bulletin*, **90,** 1641-1690.

Dickson, J. (1966) Carbonate identification and genesis as revealed by staining. *Journal of Sedimentary Research*, **36,** 491-505.

Dong, S.F., Chen, D.Z., Qing, H.R., Jiang, M.S. and Zhou, X.Q. (2013a) In situ stable isotopic constraints on dolomitizing fluids for the hydrothermally-originated saddle dolomites at Keping, Tarim Basin. *Chinese Science Bulletin*, **58,** 2877-2882.

Dong, S.F., Chen, D.Z., Qing, H.R., Zhou, X.Q., Wang, D., Guo, Z.H., Jiang, M.S. and Qian, Y.X. (2013b) Hydrothermal alteration of dolostones in the Lower Ordovician, Tarim Basin, NW China: Multiple constraints from petrology, isotope geochemistry and fluid inclusion microthermometry. *Marine and Petroleum Geology*, **46,** 270-286.

Ehrenberg, S.N., Eberli, G.P., Keramati, M. and Moallemi, S.A. (2006) Porosity-permeability relationships in interlayered limestone-dolostone reservoirs. *American Association of Petroleum Geologists, Bulletin*, **90,** 91-114.

Ehrenberg, S.N., Walderhaug, O. and Bjørlykke, K. (2012) Carbonate porosity creation by mesogenetic dissolution: Reality or illusion? *American Association of Petroleum Geologists, Bulletin*, **96,** 217-233.

Friedman, I. and O'Neil, J.R. (1977) *Compilation of stable isotope fractionation factors of geochemical interest*. USGPO.

Goldstein, R.H. and Reynolds, T.J. (1994) Systematics of fluid inclusions in diagenetic minerals: SEPM Short Course Notes, 31. 199.

Gomez-Rivas, E., Corbella, M., Martín-Martín, J., Stafford, S., Teixell, A., Bons, P., Griera, A. and Cardellach, E. (2014) Reactivity of dolomitizing fluids and Mg source evaluation of fault-controlled dolomitization at the Benicàssim outcrop analogue (Maestrat basin, E Spain). *Marine and Petroleum Geology*, **55,** 26-42.

Gregg, J.M., Bish, D.L., Kaczmarek, S.E. and Machel, H.G. (2015) Mineralogy, nucleation and growth of dolomite in the laboratory and sedimentary environment: a review. *Sedimentology*.

Haas, J., Budai, T., Győri, O. and Kele, S. (2014) Multiphase partial and selective dolomitization of Carnian reef limestone (Transdanubian Range, Hungary). *Sedimentology*, **61,** 836-859.

Heydari, E. (1997) The role of burial diagenesis in hydrocarbon destruction and H2S accumulation, upper Jurassic Smackover Formation, Black Creek Field, Mississippi. *American Association of Petroleum Geologists Bulletin*, **81,** 26-45.

Hiemstra, E.J. and Goldstein, R.H. (2015) Repeated injection of hydrothermal fluids into downdip carbonates: a diagenetic and stratigraphic mechanism for localization of reservoir porosity, Indian Basin Field, New Mexico, USA. *Geological Society, London, Special Publications*, **406,** 141-177.

Hugman III, R. and Friedman, M. (1979) Effects of texture and composition on mechanical behavior of experimentally deformed carbonate rocks. *American Association of Petroleum Geologists, Bulletin*, **63,** 1478-1489.

Jiang, L., Cai, C.F., Worden, R.H., Li, K.K. and Xiang, L. (2013) Reflux dolomitization of the Upper Permian Changxing Formation and the Lower Triassic Feixianguan Formation, NE Sichuan Basin, China. *Geofluids*, **13,** 232-245.

Jiang, L., Cai, C.F., Worden, R.H., Li, K.K., Xiang, L., Chu, X.L., Shen, A.J. and Li, W.J. (2015a) Rare earth element and yttrium (REY) geochemistry in carbonate reservoirs during deep burial diagenesis: Implications for REY mobility during thermochemical sulfate reduction. *Chemical Geology*, **415,** 87-101.

Jiang, L., Pan, W.Q., Cai, C.F., Jia, L.Q., Pan, L.Y., Wang, T.K., Li, H.X., Chen, S.L. and Chen, Y. (2015b) Fluid mixing induced by hydrothermal activity in the Ordovician carbonates in Tarim Basin, China. *Geofluids*, **15,** 483-498.

Jiang, L., Worden, R.H. and Cai, C.F. (2014a) Thermochemical sulfate reduction and fluid evolution of the Lower Triassic Feixianguan Formation sour gas reservoirs, northeast Sichuan Basin, China. *American Association of Petroleum Geologists, Bulletin*, **98,** 947-973.

Jiang, L., Worden, R.H. and Cai, C.F. (2015c) Generation of isotopically and compositionally distinct water during thermochemical sulfate reduction (TSR) in carbonate reservoirs: Triassic Feixianguan Formation, Sichuan Basin, China. *Geochimica et Cosmochimica Acta*, **165,** 249-262.

Jiang, L., Worden, R.H., Cai, C.F., Li, K.K., Xiang, L., Cai, L.L. and He, X.Y. (2014b) Dolomitization of Gas Reservoirs: The Upper Permian Changxing and Lower Triassic Feixianguan Formations, Northeast Sichuan Basin, China. *Journal of Sedimentary Research*, **84,** 792-815.

Jones, G.D., Smart, P.L., Whitaker, F.F., Rostron, B.J. and Machel, H.G. (2003) Numerical modeling of reflux dolomitization in the Grosmont platform complex (Upper Devonian), Western Canada sedimentary basin. *American Association of Petroleum Geologists, Bulletin*, **87,** 1273-1298.

Jones, G.D. and Xiao, Y. (2005) Dolomitization, anhydrite cementation, and porosity evolution in a reflux system: Insights from reactive transport models. *American Association of Petroleum Geologists, Bulletin*, **89,** 577.

Kinsman, D.J. (1966) Gypsum and anhydrite of recent age, Trucial Coast, Persian Gulf. In: *Second symposium on salt*, **1**, pp. 302-326. Northern Ohio Geol. Soc Cleveland, OH.

Land, L.S. (1983) The application of stable isotopes to studies of the origin of dolomite and to problems of diagenesis of clastic sediments. *Stable isotopes in sedimentary geology: SEPM Short Course*, **10,** 4-1.

Liu, Z.B., Yang, S.B., Jiao, C.L., Cai, X.R., Yan, X.J. and Wang, E.H. (2012) High resolution sequence stratigraphy and sedimentary characteristics of the Middle-Lower Cambrian in Bachu Uplift, the Tarim Basin. *Oil & Gas Geology*, **33,** 70-76.

Machel, H.G. (2004) Concepts and models of dolomitization: a critical reappraisal. *The geometry and petrogenesis of dolomite hydrocarbon reservoirs***,** 7¨C63.

Machel, H.G. and Lonnee, J. (2002) Hydrothermal dolomite--a product of poor definition and imagination. *Sedimentary Geology*, **152,** 163-171.

Machel, H.G., Sumrall, J.B., Kambesis, P.N., Mylroie, J.R., Mylroie, J.E. and Lace, M.J. (2014) Episodic Fluid Flow and Dolomitization By Methane-Bearing Pore Water of Marine Parentage In An Accretionary Prism Setting, Barbados, West Indies. *Journal of Sedimentary Research*, **84,** 58-71.

Martín-Martín, J., Travé, A., Gomez-Rivas, E., Salas, R., Sizun, J.-P., Vergés, J., Corbella, M., Stafford, S. and Alfonso, P. (2015) Fault-controlled and stratabound dolostones in the Late Aptian–earliest Albian Benassal Formation (Maestrat Basin, E Spain): Petrology and geochemistry constrains. *Marine and Petroleum Geology*, **65,** 83-102.

Melim, L.E., Swart, P.S. and Maliva, R.G. (2001) Meteoric and marine-burial diagenesis in the subsurface of Great Bahama Bank: Results of the Bahamas Drilling Project (Ed R.N. Ginsburg). *SEPM Spec. Publ.*, **70,** 137-161.

Montañez, I.P., Banner, J.L., Osleger, D.A., Borg, L.E. and Bosserman, P.J. (1996) Integrated Sr isotope variations and sea-level history of Middle to Upper Cambrian platform carbonates: Implications for the evolution of Cambrian seawater 87Sr/86Sr. *Geology*, **24,** 917-920.

Montañez, I.P., Osleger, D.A., Banner, J.L., Mack, L.E. and Musgrove, M. (2000) Evolution of the Sr and C isotope composition of Cambrian oceans. *GSA today*, **10,** 1-7.

Oakes, C.S., Bodnar, R.J. and Simonson, J.M. (1990) The system NaCl-$CaCl_2$-H_2O: I. the ice liquidus at 1 atm total pressure. *Geochemica et Cosmochimica Acta*, **54,** 603-611.

Qing, H.R. and Mountjoy, E.W. (1994) Formation of coarsely crystalline, hydrothermal dolomite reservoirs in the Presqu'ile barrier, Western Canada Sedimentary Basin. *American Association of Petroleum Geologists, Bulletin*, **78,** 55-77.

Qiu, N.S., Chang, J., Zuo, Y.H., Wang, J.Y. and Li, H.L. (2012) Thermal evolution and maturation of lower Paleozoic source rocks in the Tarim Basin, northwest China. *American Association of Petroleum Geologists, Bulletin*, **96,** 789-821.

Rosenbaum, J. and Sheppard, S. (1986) An isotopic study of siderites, dolomites and ankerites at high temperatures. *Geochimica et Cosmochimica Acta*, **50,** 1147-1150.

Saller, A.H. and Dickson, J.A.T.D. (2011) Partial dolomitization of a Pennsylvanian limestone buildup by hydrothermal fluids and its effect on reservoir quality and performance. *American Association of Petroleum Geologists, Bulletin*, **95,** 1745-1762.

Saller, A.H., Pollitt, D. and Dickson, J. (2014) Diagenesis and porosity development in the First Eocene reservoir at the giant Wafra Field, Partitioned Zone, Saudi Arabia and Kuwait. *American Association of Petroleum Geologists, Bulletin*, **98,** 1185-1212.

Schmoker, J.W. and Halley, R.B. (1982) Carbonate porosity versus depth: a predictable relation for south Florida. *American Association of Petroleum Geologists, Bulletin*, **66,** 2561-2570.

Sibley, D.F. (1980) Climatic control of dolomitization, Seroe Domi Formation (Pliocene), Bonaire, NA. *Soc. Econ. Paleontologists Mineralogists Spec. Publ.*, **28,** 247-258.

Smith, L.B. (2006) Origin and reservoir characteristics of Upper Ordovician Trenton–Black River hydrothermal dolomite reservoirs in New York. *American Association of Petroleum Geologists, Bulletin*, **90,** 1691-1718.

Sun, S.Q. (1995) Dolomite reservoirs: porosity evolution and reservoir characteristics. *American Association of Petroleum Geologists, Bulletin*, **79,** 186-204.

Vasconcelos, C., McKenzie, J.A., Bernasconi, S., Grujic, D. and Tiens, A.J. (1995) Microbial mediation as a possible mechanism for natural dolomite formation at low temperatures. *Nature*, **377,** 220-222.

Vasconcelos, C., McKenzie, J.A., Warthmann, R. and Bernasconi, S.M. (2005) Calibration of the δ18O paleothermometer for dolomite precipitated in microbial cultures and natural environments. *Geology*, **33,** 317-320.

Veizer, J., Ala, D., Azmy, K., Bruckschen, P., Buhl, D., Bruhn, F., Carden, G.A.F., Diener, A., Ebneth, S. and Godderis, Y. (1999) 87Sr/86Sr, δ13C and δ18O evolution of Phanerozoic seawater. *Chemical geology*, **161,** 59-88.

Wang, Z.M., Xie, H.W., Chen, Y.Q., Qi, Y.M. and Zhang, K. (2014) Discovery and Exploration of Cambrian Subsalt Dolomite Original Hydrocarbon Reservoir at Zhongshen-1 Well in Tarim Basin. *China Petroleum Exploration*, **19,** 1-13.

Warthmann, R., Van Lith, Y., Vasconcelos, C., McKenzie, J.A. and Karpoff, A.M. (2000) Bacterially induced dolomite precipitation in anoxic culture experiments. *Geology*, **28,** 1091-1094.

Whitaker, F.F. and Xiao, Y. (2010) Reactive transport modeling of early burial dolomitization of carbonate platforms by geothermal convection. *American Association of Petroleum Geologists, Bulletin*, **94,** 889-917.

Worden, R.H. and Smalley, P.C. (1996) H2S-producing reactions in deep carbonate gas reservoirs: Khuff Formation, Abu Dhabi. *Chemical geology*, **133,** 157-171.

Worden, R.H., Smalley, P.C. and Oxtoby, N.H. (1996) The effects of thermochemical sulfate reduction upon formation water salinity and oxygen isotopes in carbonate gas reservoirs. *Geochimica et Cosmochimica Acta*, **60,** 3925-3931.

Wright, D.T. and Wacey, D. (2005) Precipitation of dolomite using sulphate‐reducing bacteria from the Coorong Region, South Australia: significance and implications. *Sedimentology*, **52,** 987-1008.

Ye, D.S. (1994) Deep dissolution of Cambrian-Ordovician carbonates in the Northern Tarim Basin. *Acta Sedimentological Sinica*, **12,** 66-71.

You, X.L., Sun, S., Zhu, J.Q., Li, Q., Hu, W.X. and Dong, H.L. (2013) Microbially mediated dolomite in Cambrian stromatolites from the Tarim Basin, north‐west China: implications for the role of organic substrate on dolomite precipitation. *Terra Nova*, **25,** 387-395.

Zengler, D.H., Dunham, J.D. and Ethington, R.L. (1980) Concepts and models of dolomitization. *SEPM Special Publication*, **28,** 320 p.

Zhang, Y., Chen, D., Zhou, X., Guo, Z., Wei, W. and Mutti, M. (2015) Depositional facies and stratal cyclicity of dolomites in the Lower Qiulitag Group (Upper Cambrian) in northwestern Tarim Basin, NW China. *Facies*, **61,** 1-24.

Zhao, W.Z., Shen, A.J., Zhou, J.G., Wang, X.F. and Lu, J.M. (2014) Types, characteristics, origin and exploration significance of reef-shoal reservoirs: A case study of Tarim Basin, NW China and Sichuan Basin, SW China. *Petroleum Exploration and Development*, **41,** 257-267.

Zhao, Z.J., Luo, J.H., Zhang, Y.B., Wu, X.N. and Pan, W.Q. (2011) Lithofacies paleogeography of Cambrian sequences in the Tarim Basin. *Acta Petrolei Sinica*, **32,** 937-948.

Zheng, J.F., Shen, A.J., Liu, Y.F. and Chen, Y.Q. (2013) Main controlling factors and characteristics of Cambrian dolomite reservoirs related to evaporite in Tarim Basin. *Acta Sedimentologica Sinica*, **31,** 89-98.

Zhu, D.Y., Meng, Q.Q., Jin, Z.J., Liu, Q.Y. and Hu, W.X. (2015) Formation mechanism of deep Cambrian dolomite reservoirs in the Tarim basin, northwestern China. *Marine and Petroleum Geology*, **59,** 232-244.

FIGURE CAPTION

Figure 1. Map of the Tarim Basin showing tectonic units, locations of sampled wells and outcrops.

Figure 2. Sequence, lithology, facies, and reservoir description chart of the Cambrian strata in the Tarim Basin. Sequences and facies analysis data are modified from Zhao et al. (2011) and Liu et al. (2012).Figure 3. The cross section (from E to F in Figure 1) shows various sediment facies and lithologies of the Cambrian strata in the Tarim Basin. Modified from Zhao et al. (2011) and Liu et al. (2012).

Figure 4. East-west cross section A (from A to B in Figure 1), and north-south cross section B (from C to D in Figure 1), show the structure in different tectonic units in the Tarim Basin. A was modified from Cai et al. (2009a) , and B was modified from Zhu et al. (2015).

Figure 5. Burial histories of the Camrbian sediments in different tectonic units: (A) from TZ1 well in Tazhong Uplift; (B) from TD1 well in Tadong Uplift; (C) from H4 well in the Bachu Uplift; and (D) from Keping outcrop and Yakela subsurface in Keping Uplift. Burial histories were modified from Qiu et al. (2012) for A, B, C, and Ye (1994) for D, respectively.

Figure 6. Thin-section and CL photomicrographs show different kinds of dolomites in Cambrian strata in the Tarim Basin. A) stromatolitic laminae of alternating dark dolomudstone (red arrow) and light microsparite layers (yellow arrow), pyrite and EPS fossils (You et al., 2013) are presented in the dark dolomudstone, outcrop Xiaoerbulake, $\in_{3q}$. B) Very finely crystalline dolomicrite (D2) (in dark colour; red arrow), and the associated anhydrite nodule (in white colour) from restricted lagoon facies, well ZS5, 6435.2 m, $\in_{1w}$. C) CL photomicrograph for Part C; dolomicrite shows dull red luminescence (yellow arrow) and anhdyrite cement is nonluminescent, well ZS5, 6435.2m, $\in_{1w}$. D) Very fine-crystalline, fabric retentive dolomite (D3) with fine-crystalline, porphyrotopic dolomite (D5); the algae fabric and intercrystalline and dissolution pores (in blue) are persevered in D3; well H4, 5355.5 m, $\in_{2s}$. E) CL photomicrograph for Part E; fabric retentive dolomite shows very dull red luminescence (yellow arrow), and porphyrotopic dolomite shows slightly lighter but also dull red luminescence (red yellow), well H4, 5355.5 m, $\in_{2s}$. F) Medium-coarse crystalline, planar-s to nonplanar-a, fabric obliterative dolomicrite (D4) with some dolomite cements (D5) grow at the eage of intergranular pores (blue colour; red arrow), bitumen (black colour) and quatz cement (white colour) fill some of the porosity, the primary fabric has been obliterated due to intense dolomitization and recrystallization, well ZS5, 6280.0 m, $\in_{2s}$. G) CL photomicrograph for Part A; D4 shows very dull red luminescence (yellow arrow), while D5 show light orange luminescence, well ZS5, 6280.0 m, $\in_{2s}$. H) coarse -crystalline fabric obliterative crystalline dolomicrite (D4), with coarse-crystalline dolomite cement (D5) grow in to vugs which was filled by calcite cement, well TZ75, 4815.7 m, $\in_{1x}$. I) CL photomicrograph for Part C; D4 z show dull red luminescence, D5 shows light orange luminescence, and calcite cement is nonluminescent , well TZ75, 4815.7 m, $\in_{3q}$. J) Coarse-crystalline, fracture filling, saddle dolomite (D6), characterized by curved crystal faces and undulose extinction, outcrop Xiaoerbulake, $\in_{1x}$. K) CL photomicrograph for Part G; saddle dolomite shows orange luminescence, outcrop Xiaoerbulake, $\in_{1x}$. L)

A BSEM image showing the growth of pyrite (Py) in the intergranular pores in fabric oblitertive dolomites, well ZS5, 6280.0 m, $\in_{2s}$.

Figure 7. Photomicrographs showing different diagenetic minerals in addition to dolomite in the Cambrian dolostone reservoirs in the Tarim Basin. (A) Fracture filling anhydrite cements (red arrow) in dolomicrite (D1), well ZS5, 6434.31 m, $\in_{1w}$. (B) Anhydrite nodule/cements (red arrow) growth associted with chalcedony (yellow arrow), well ZS5, 6293.28 m, $\in_{2a}$. (C) Fracture/vug filling coarsely crystalline quartz cement (yellow arrow), outcrop Xiaoerbulake, $\in_{3q}$. (D) Fracture filling coarsely crystalline calcite cement (red arrow), outcrop Xiaoerbulake, $\in_{1w}$. (E) Vug filling coarsely crystalline calcite cements, well TZ75, 4836.5 m, $\in_{3q}$. (F) A BSEM image showing a fracture filling hydrothermal mineral assemblage of sphalerite, barite, and calcite, well TZ104, 3755.6 m, $\in_{3q}$.

Figure 8. Photomicrographs show different pore types in the Cambrian dolostone reservoirs in the Tarim Basin. (A) Enlarged intragranular pore (blue colour; red arrow) preserved in dolomicrite (D2), well H4, 5355.5 m, $\in_{2s}$. (B) Intercrystalline pore (blue colour; red arrow) presevered in fine-crystalline fabric retentive dolomite (D3), with bitumen (black colour) fillings, well H4, $\in_{2s}$. (C) Disslusion and modic pores (red arrow) were found in fabric obliterative dolomicrite (D4), outcrop Xiaoerbulake, $\in_{3q}$. (D) Enlarged intergranular pores (blue colour; red arrow) are well developed in fabric obliterative dolomicrite (D4), with bitumen (black colour) and quatz cement (white colour) fillngs, well ZS5, 6280.0 m, $\in_{2s}$. (E) Late diagenetic, big dissolution pores (red arrow) persevered in fracture filling saddle dolomite (D6); outcrop Xiaoerbulake, $\in_{1x}$. (F) Late diagenetic, big dissolution pores (red arrow) persevered in vug filling calcite; well TZ166, 6071.1 m, $\in_{1q}$. (G) Suprastratal deformation generated fractures (red arrow) and pores in dolomicrite and anhydrite breccias, with bitumen (black colour) fillings locally presented, well ZS5, 6193.3 m, $\in_{2a}$. (H) Late diagenetic disslution pores (red arrow) likely related to hydrothermal dolomitization and fluids mixing, well TS1, 8400.0m, $\in_{3q}$.

Figure 9. Paragenetic sequence of the Cambrian unite in the Tarim Basin summarizing major products of seawater, near-surface, shallow-burial, mesogenetic to deep burial, uplift diagenesis, and their effect on reservoir porosiy and permeability. Por stands for Porosity; Perm stands for Permeability; Grey rectangles represent different types of dolomites; open rectangles represent different dissolution and fracturing events; black rectangles represent all the other diagenetic events.

Figure 10. Fluid inclusion data from fabric obliterative dolomite (D4), medium to coarse dolomite cement (D5), and saddle dolomite cement (D6) in the Cambrian strata, Tarim Basin. The data show that these dolomites are formed in high-salinity formation water at relatively higher temperatures.

Figure 11. Salinities of two-phase aqueous fluid inclusions in fabric obliterative dolomite (D4) and medium to coarse dolomite cement (D5) are significantly lower than the one in saddle dolomite cement (D6). There is lacking of relationship between temperature and salinity.

Figure 12. Carbon and oxygen-isotope compositions and ranges of various types of dolomites from the Cambrian strata in the Tarim Basin, marking with lines show different colours and styles. The coeval

seawater isotopic range is marked with blue bars, data from Montañez et al. (2000) and Veizer et al. (1999).

Figure 13. $^{87}Sr/^{86}Sr$ ratios of various types of dolomites in the Cambrian strata, Tarim Basin. Coeval seawater $^{87}Sr/^{86}Sr$ data marked in blue bar are from Montañez et al. (1996), Montañez et al. (2000) and Veizer et al. (1999).

Figure 14. Schematic diagram of the dolostone paragenesis in the Cambrian strata in the Tarim Baisn. The diagram showing diffenrent dolomitization models with different dolomitization fluids, temperature and dolomite types.

Figure 15. Temperature vs. $\delta^{18}O$ diagenetic fluid for various $\delta^{18}O$ dolomite values that were reconstructed from the equation $10^3 \ln\alpha = 3.2 \times 10^6/T^{-2}–3.3$ (Land, 1983). Red and blue shaded areas mark the preferred temperature ranges for saddle dolomite and deep burial diagenetic dolomites (fabric-obliterative dolomite, porphyrotopic dolomite, and dolomite cement), whereas green, orange and yellow shaded areas mark the preferred temperature ranges for low temperature microbial dolomite, reflux dolomite (dolomicrite and fabric-retentive dolomite) and seawater dolomite (fabric-retentive dolomite), respectively.

TABLE CAPTION

Table 1. $\delta^{13}C$, $\delta^{18}O$, and $^{87}Sr/^{86}Sr$ isotopic values of various types of dolomite in the Cambrian strata in the Tarim Basin.

Table 2. Summary of the key attributes of different types of dolostones found in the Cambrian strata in the Tarim Basin.

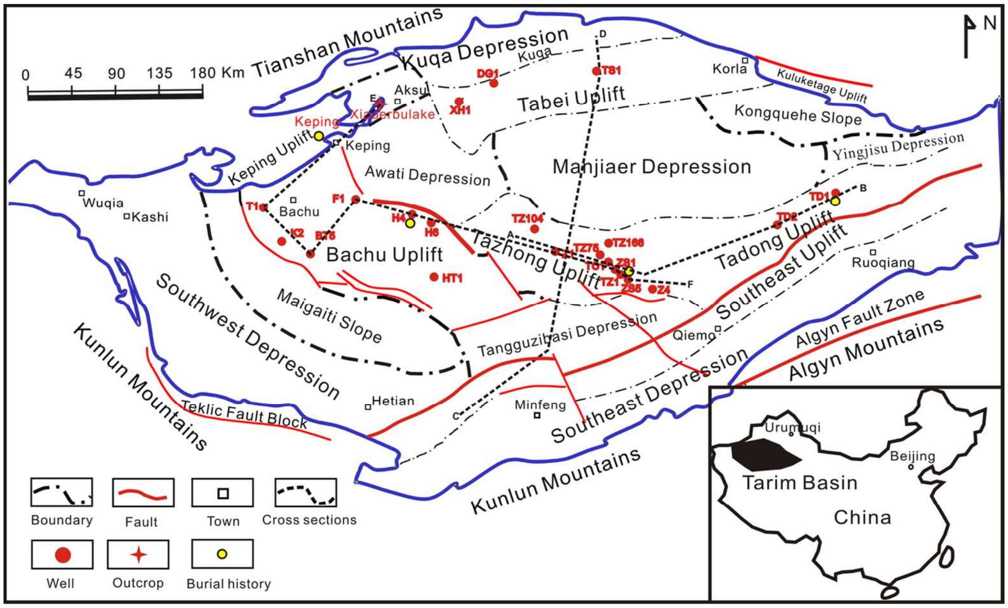

127x76mm (300 x 300 DPI)

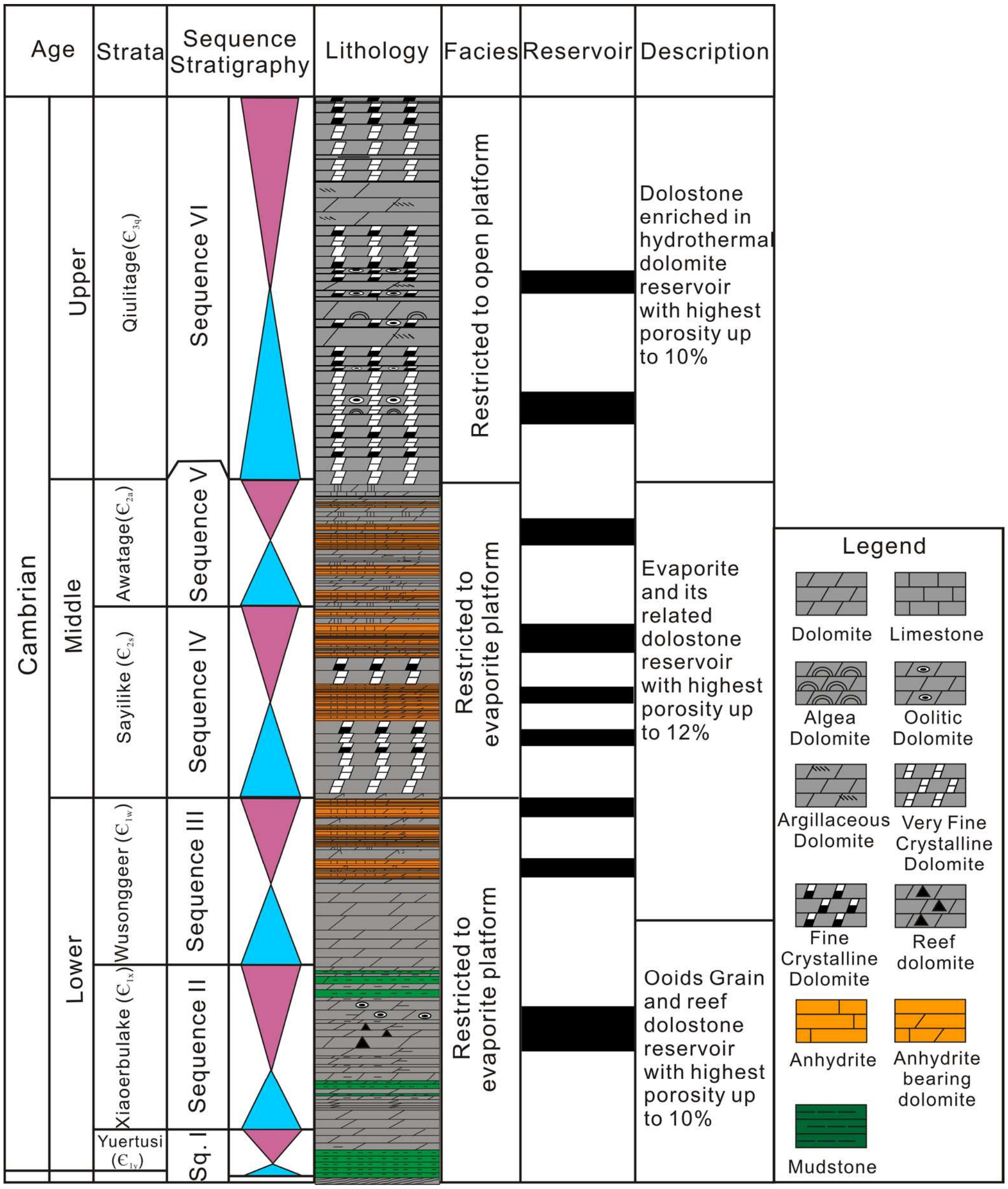

178x211mm (300 x 300 DPI)

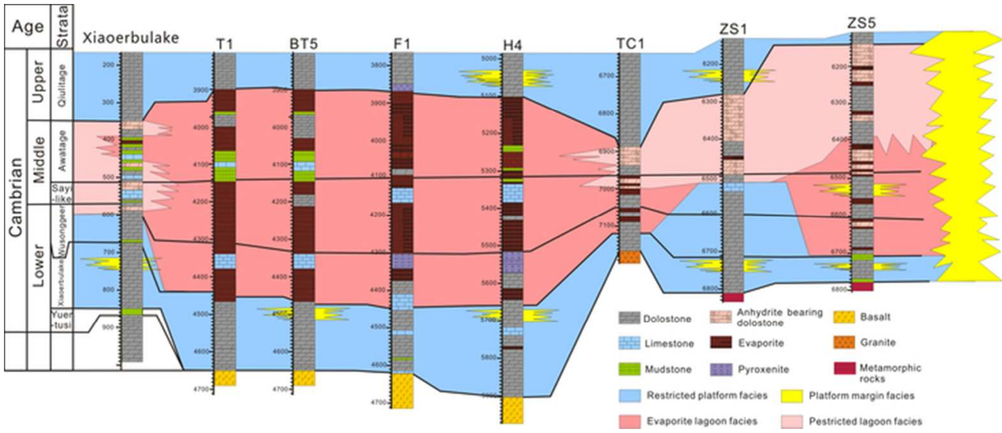

61x26mm (300 x 300 DPI)

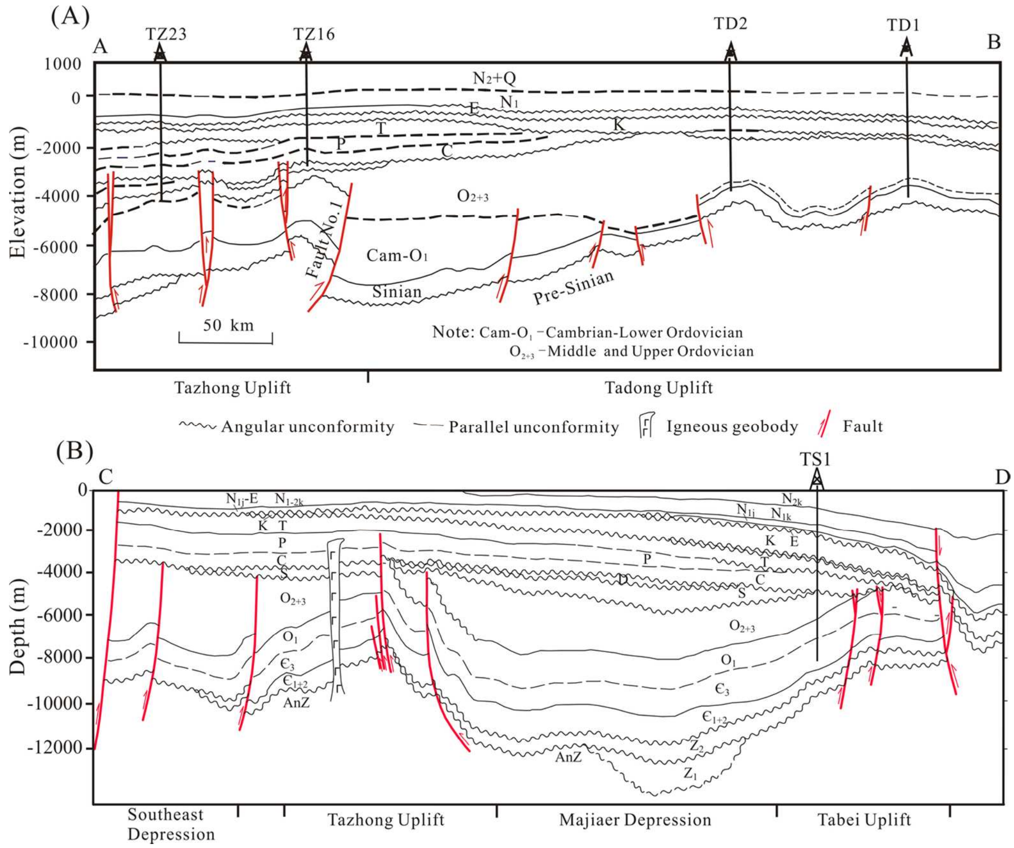

133x112mm (300 x 300 DPI)

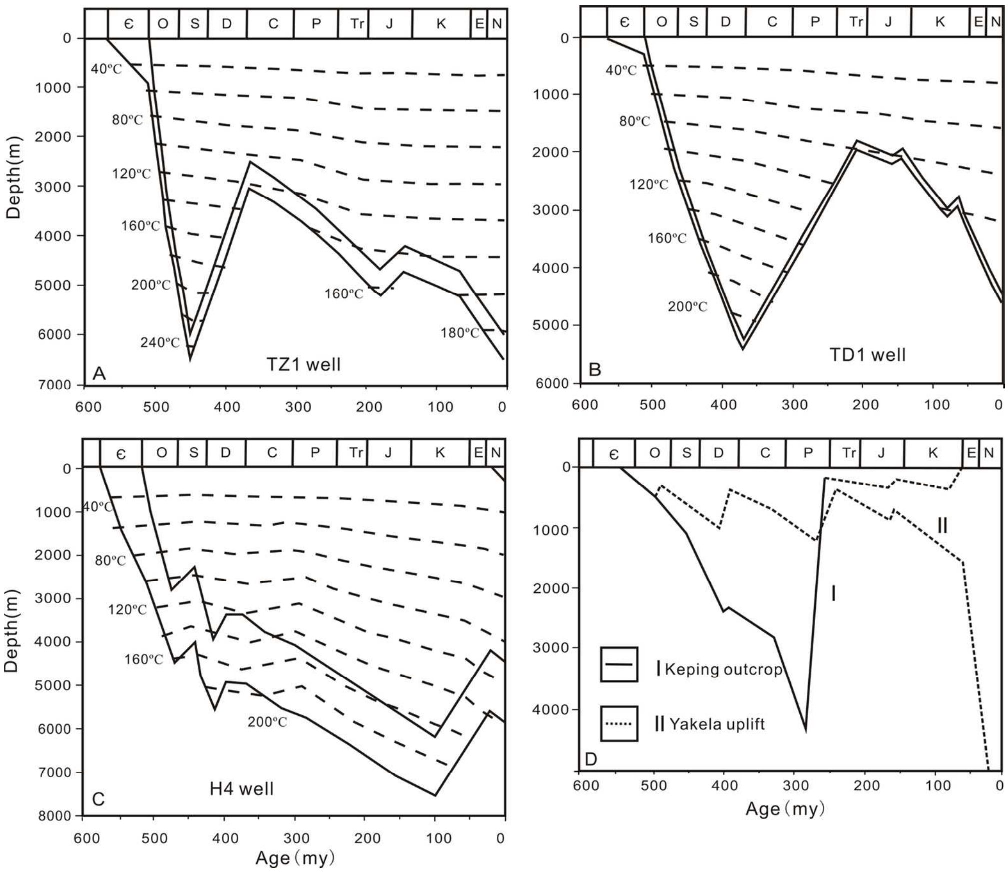

132x114mm (300 x 300 DPI)

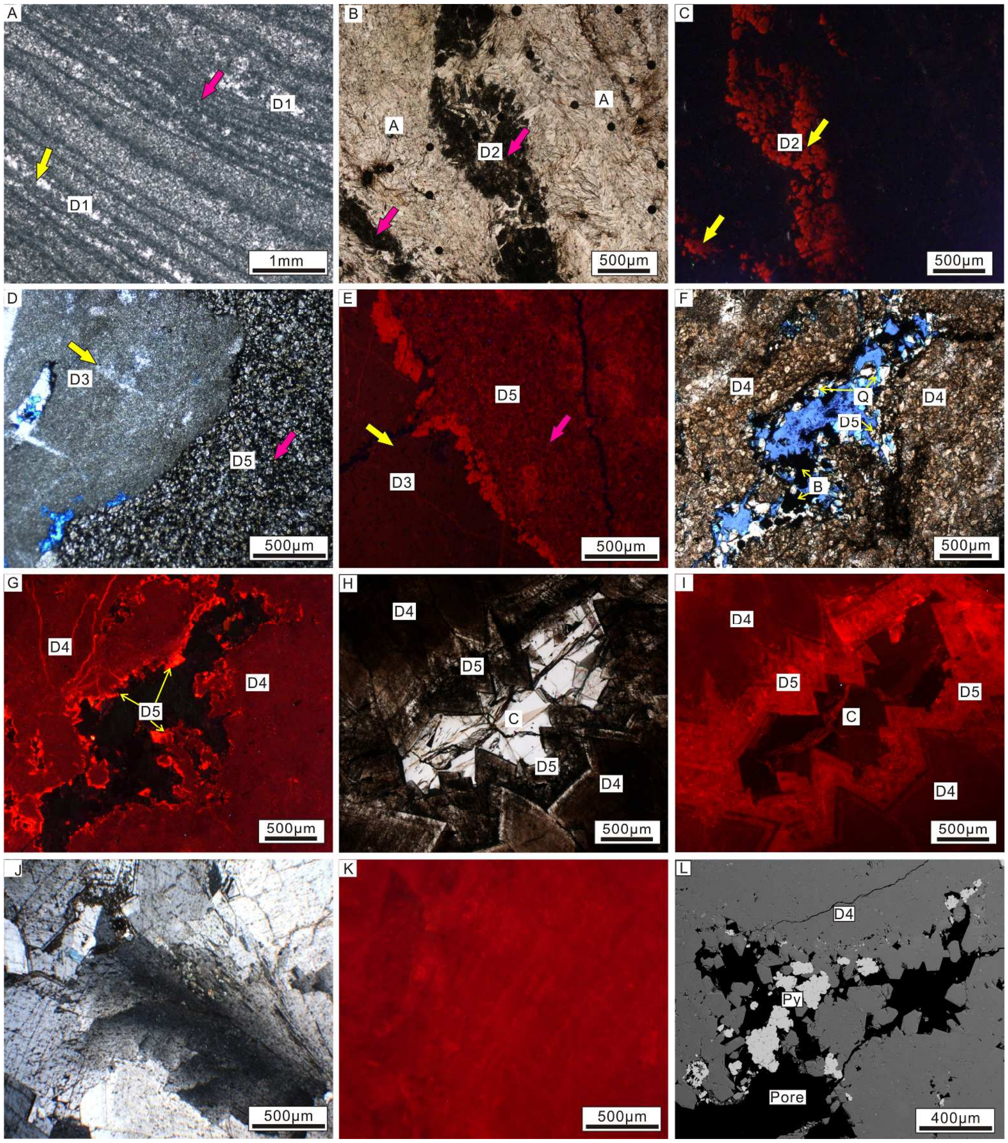

268x304mm (300 x 300 DPI)

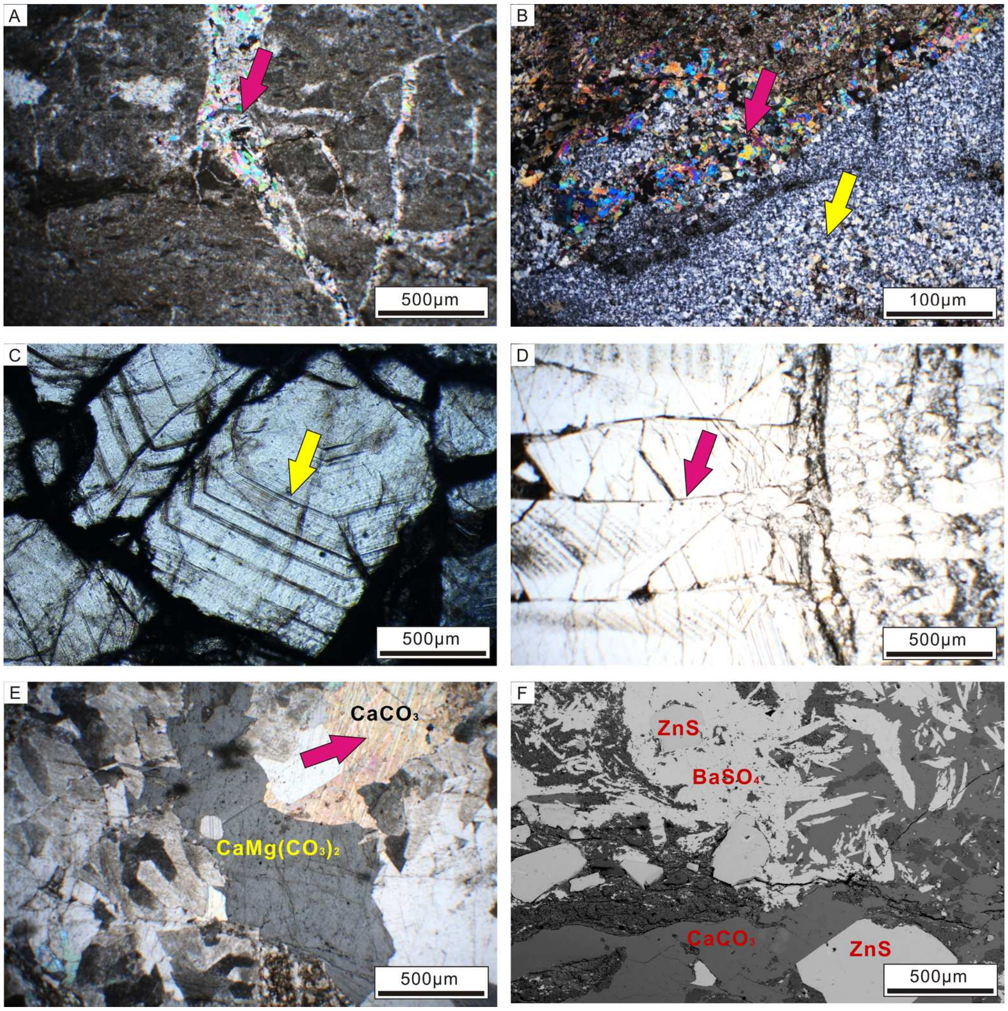

203x204mm (300 x 300 DPI)

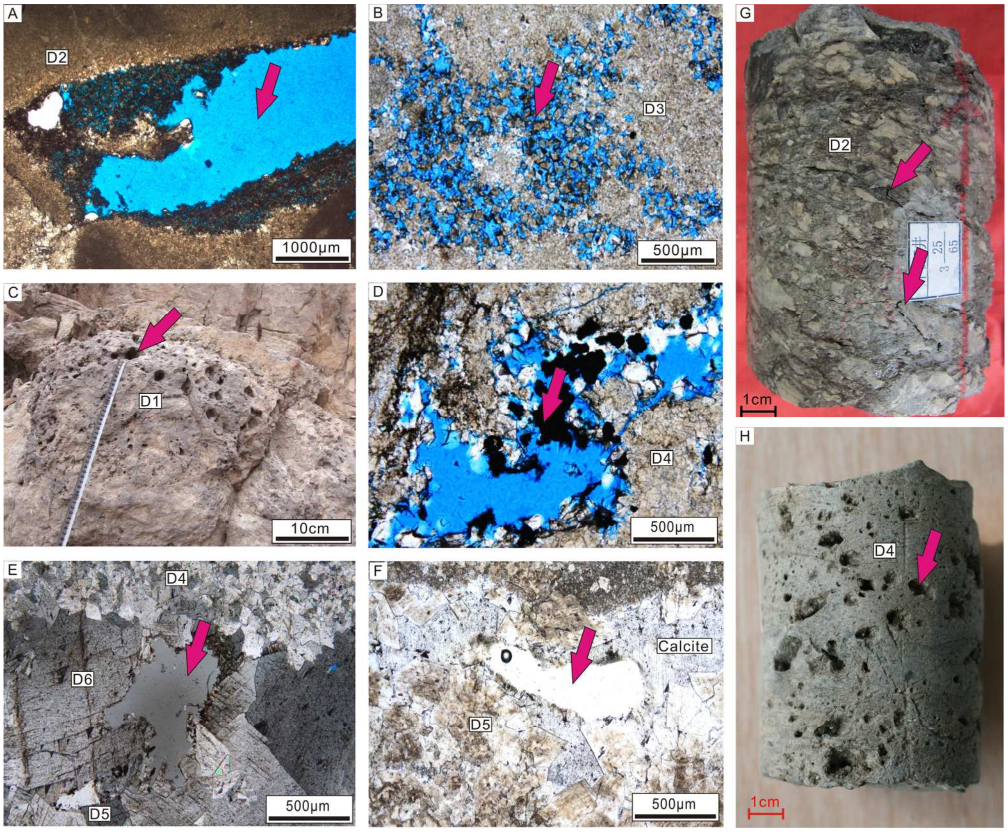

194x160mm (300 x 300 DPI)

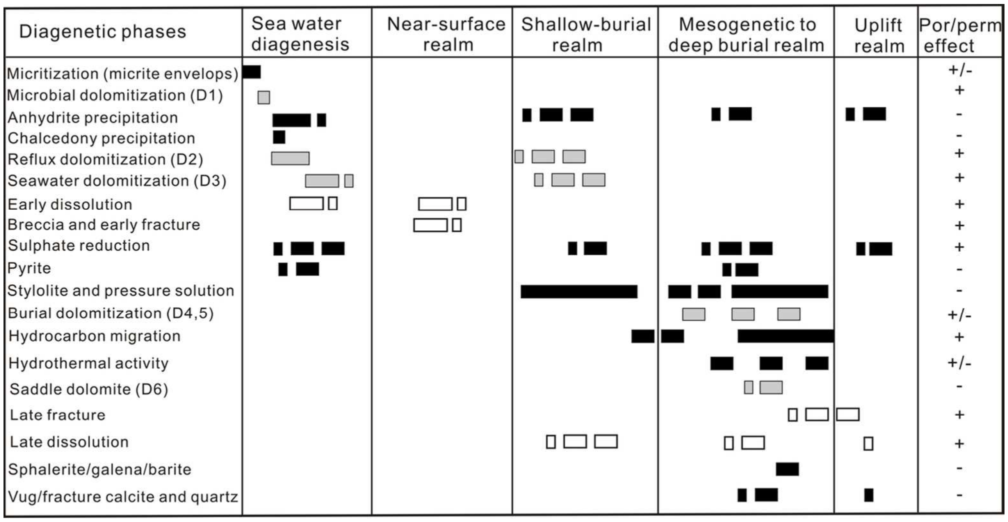

117x60mm (300 x 300 DPI)

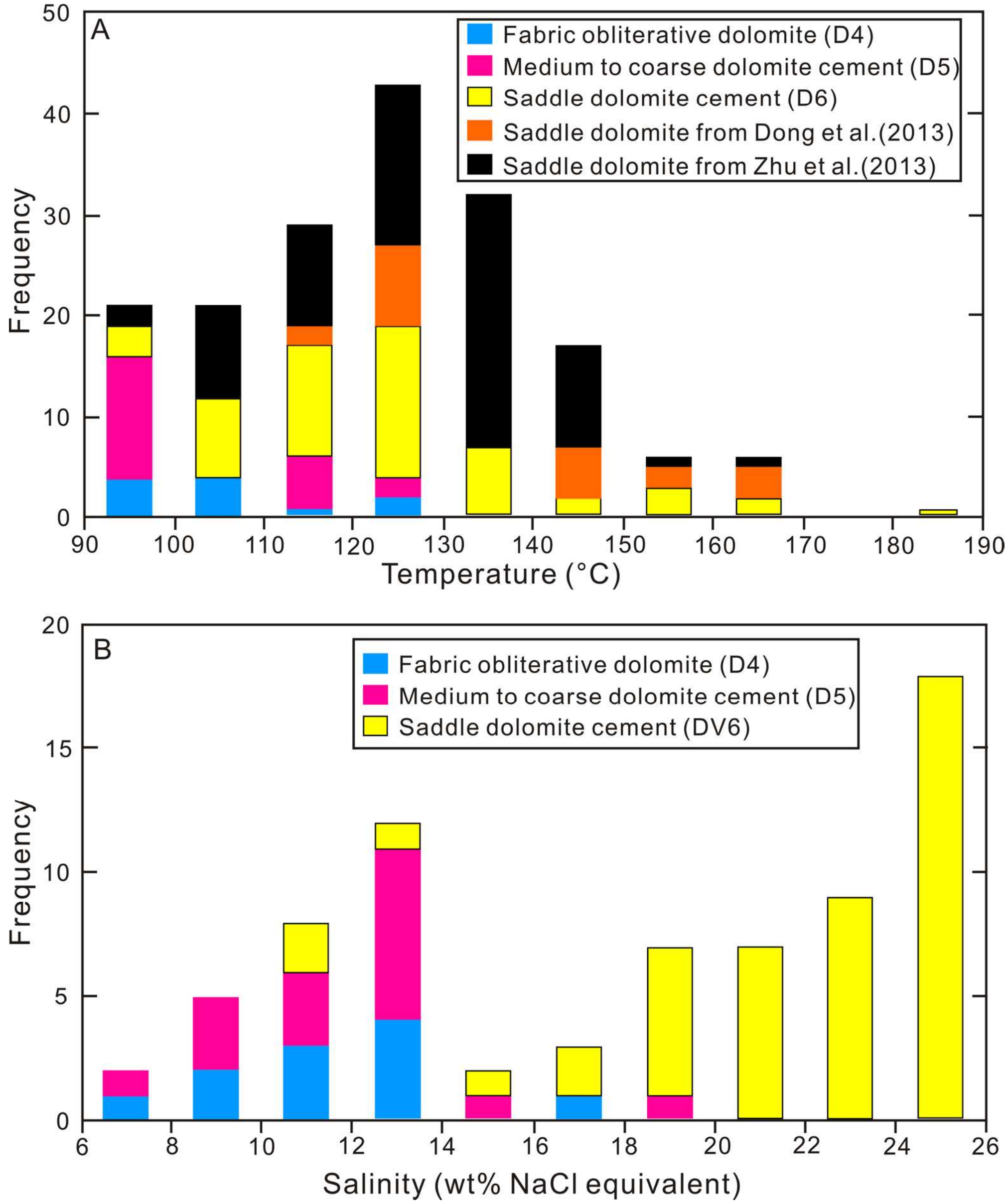

177x213mm (300 x 300 DPI)

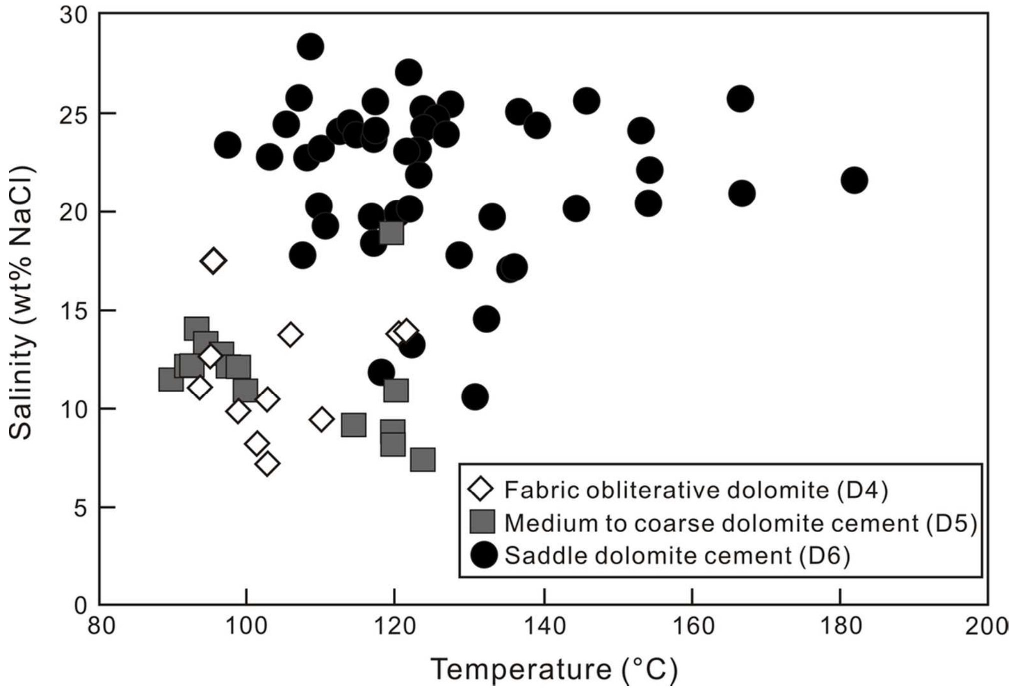

97x66mm (300 x 300 DPI)

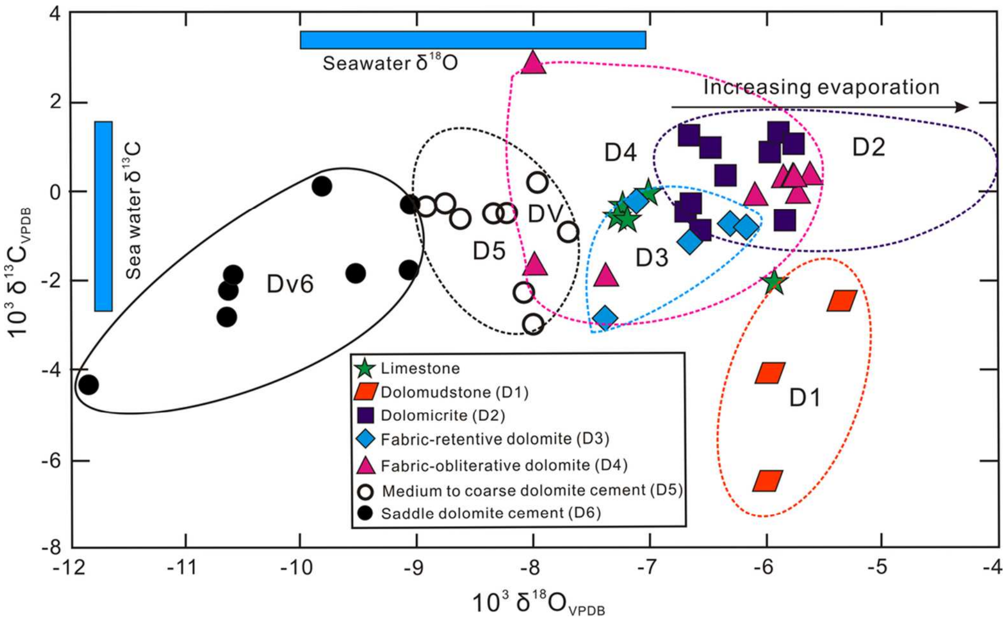

101x62mm (300 x 300 DPI)

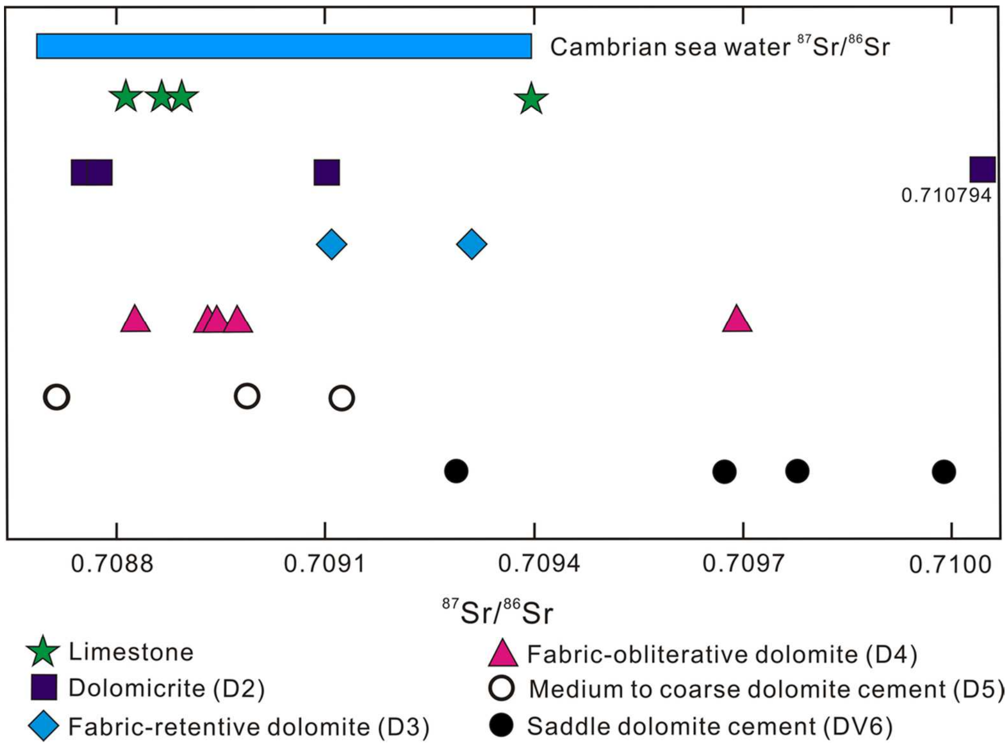

104x76mm (300 x 300 DPI)

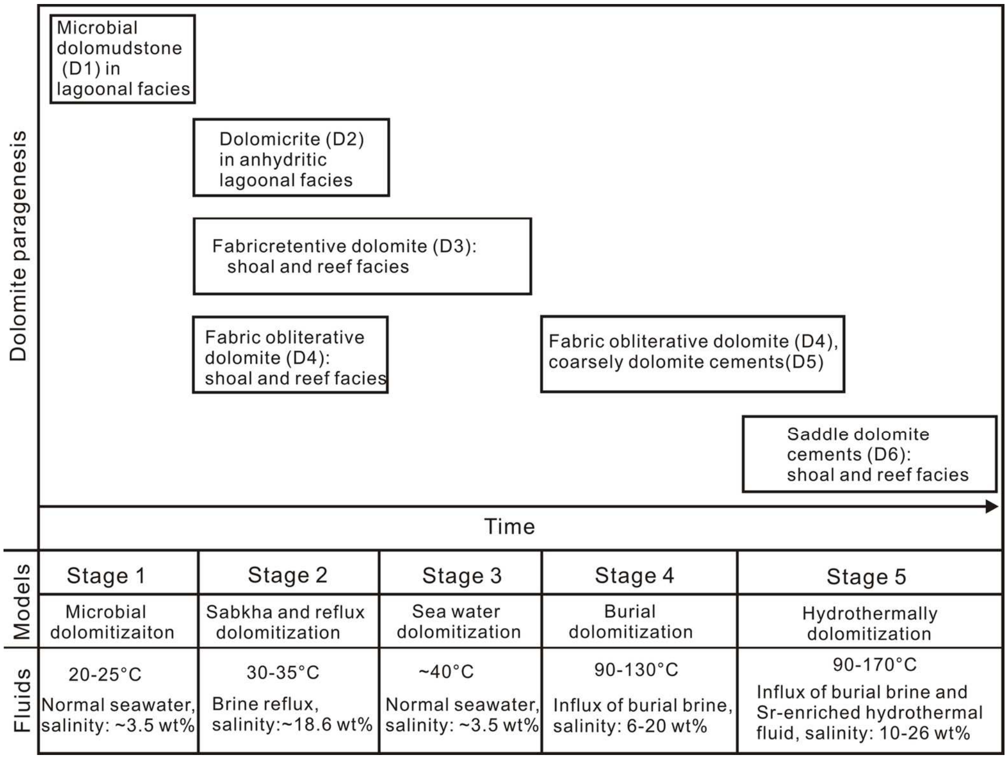

145x109mm (300 x 300 DPI)

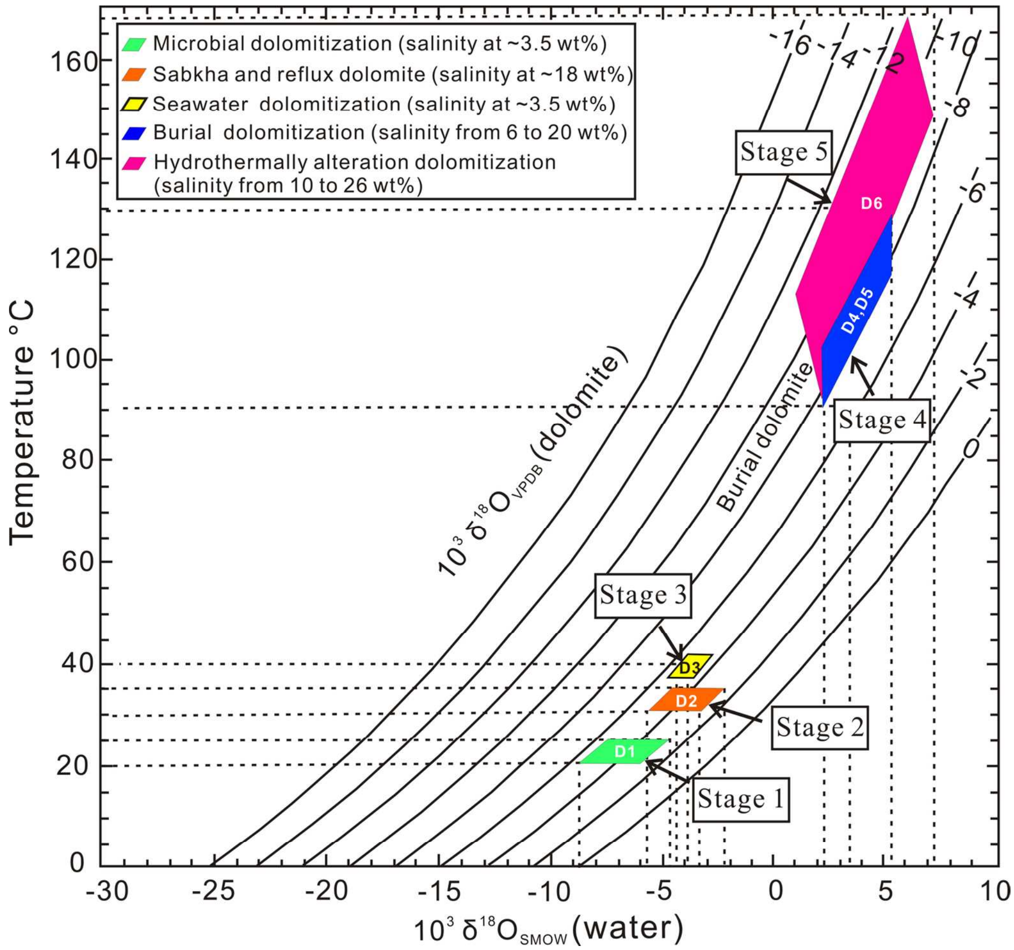

142x133mm (300 x 300 DPI)

Table 1

Samples	Depth (m)	Fm.	Description wafer	$10^3\delta^{18}O_{VPDB}$	$10^3\ \delta^{13}C_{VPDB}$	$^{87}Sr/^{86}Sr$	Error (2s)
TZ104-4-2	3706.2	∈3q	Limestone	-5.92	-2.06	0.709395	0.000011
H4 34 14/74	--	∈2s	Limestone	-7.01	0.01	0.708893	0.000009
H4 34 25/74	--	∈2s	Limestone	-7.3	-0.6	--	--
H4 34 32/74	--	∈2s	Limestone	-7.23	-0.3	0.708814	0.000009
H4 34 71/74	5355.5	∈2s	Limestone	-7.19	-0.64	0.708865	0.00001
S1-1-10	6713.3	∈1x	Dolomudstone (D1)	-5.96	-4.05	--	--
ZS1-1-27	--	∈1x	Dolomudstone (D1)	-5.98	-6.46	--	--
TZ75-28-13/55	4939.4	∈3q	Dolomudstone (D1)	-5.35	-2.46	--	--
ZS5 6-6	6434.31	∈1w	Dolomicrite (D2)	-6.34	0.37	--	--
ZS5 7-9	6535.64	∈1w	Dolomicrite (D2)	-6.7	-0.43	--	--
ZS5 7-13	6535.97	∈1w	Dolomicrite (D2)	-6.64	-0.28	--	--
ZS5 9-48	6557.17	∈1w	Dolomicrite (D2)	-6.56	-0.87	--	--
ZS5 1-13	6176.1	∈2a	Dolomicrite (D2)	-5.9	1.32	0.708755	0.000012
ZS5 3-15	6191.7	∈2a	Dolomicrite (D2)	-5.77	1.07	0.709102	0.000011
ZS5 3-29	6195.3	∈2a	Dolomicrite (D2)	-5.96	0.89	--	--
ZS5 4-18	6222.2	∈2a	Dolomicrite (D2)	-6.47	0.98	0.708776	0.00001
ZS5 10-16	6596.08	∈1w	Dolomicrite (D2)	-6.66	1.27	--	--
ZS5 11-31	6708.41	∈1x	Dolomicrite (D2)	-5.83	-0.66	0.710794	0.000009
TZ104-8-9/30	3756.8	∈3q	Fabric retentive dolomite (D3)	-7.38	-2.79	--	--
X-24	Outcrop	∈2a	Fabric retentive dolomite (D3)	-7.11	-0.18	--	--
X-25	Outcrop	∈2a	Fabric retentive dolomite (D3)	-6.66	-1.04	--	--
X-28	Outcrop	∈3q	Fabric retentive dolomite (D3)	-6.17	-0.71	0.709109	--
X-33	Outcrop	∈3q	Fabric retentive dolomite (D3)	-6.31	-0.65	0.709314	--
ZS5 5-4	6280.28	∈2s	Fabric obliterative dolomite (D4)	-5.72	-0.02	0.708973	0.00001
ZS5 5-15	6281.37	∈2s	Fabric obliterative dolomite (D4)	-6.09	-0.1	--	--
ZS5 5-19	6281.7	∈2s	Fabric obliterative dolomite (D4)	-5.77	0.37	--	--
ZS5 5-20	6281.85	∈2s	Fabric obliterative dolomite (D4)	-5.75	0.32	--	--
ZS5 5-25	6282.1	∈2s	Fabric obliterative dolomite (D4)	-5.63	0.39	0.708931	0.000009
ZS5 5-30	6282.36	∈2s	Fabric obliterative dolomite (D4)	-5.85	0.3	--	--
X-12	Outcrop	∈1x	Fabric obliterative dolomite (D4)	--	--	0.708972	0.000013
X-15	Outcrop	∈1x	Fabric obliterative dolomite (D4)	-8.01	2.89	0.708825	0.000011
TZ75-22-48	4800.9	∈3q	Fabric obliterative dolomite (D4)	-7.38	-1.9	0.708943	0.000012
TZ75-25-56	4828.4	∈3q	Fabric obliterative dolomite (D4)	--	--	0.70969	0.00001
TZ75-26-43	4836.5	∈3q	Fabric obliterative dolomite (D4)	-7.99	-1.71	0.708944	0.000009
TZ166-17-47-3	6071.1	∈3q	Medium to coarse dolomite cement (D5)	-7.7	-0.87	0.708715	0.00001
TZ75-26-43	4836.5	∈3q	Medium to coarse dolomite cement (D5)	-8.09	-2.27	0.708988	0.000012
H4 34 14/74	--	∈2s	Medium to coarse dolomite cement (D5)	-7.97	0.19	--	--
H4 34 25/74	--	∈2s	Medium to coarse dolomite cement (D5)	-8.65	-0.59	--	--
H4 34 32/74	--	∈2s	Medium to coarse dolomite cement (D5)	-8.77	-0.27	--	--
H4 34 71/74	5355.5	∈2s	Medium to coarse dolomite cement (D5)	-8.24	-0.55	--	--
TZ166-17-47-3	6071.1	∈3q	Medium to coarse dolomite cement (D5)	-8.32	-0.48	--	--
TZ166-17-57	--	∈3q	Medium to coarse dolomite cement (D5)	-8.93	-0.35	0.708711	0.000009
TZ75-23-56	4809.8	∈3q	Medium to coarse dolomite cement (D5)	-7.99	-2.97	0.709124	0.000011
TZ75-27-11	4892.2	∈3q	Saddle dolomite cement (D6)	-10.65	-2.78	0.709287	0.000022
TZ104-8-9	3756.8	∈3q	Saddle dolomite cement (D6)	-9.07	-1.75	--	--
TZ166-17-47-1	6071.1	∈3q	Saddle dolomite cement (D6)	-9.06	-0.28	--	--
TZ104-8-1	3755.5	∈3q	Saddle dolomite cement (D6)	-9.53	-1.83	0.709776	0.000011
TZ104-8-17	3757.7	∈3q	Saddle dolomite cement (D6)	-10.59	-1.87	--	--
X-8	Outcrop	∈1x	Saddle dolomite cement (D6)	-9.82	0.14	0.709672	0.000013
X-12	Outcrop	∈1x	Saddle dolomite cement (D6)	-11.83	-4.33	0.709989	0.000014
X-15	Outcrop	∈1x	Saddle dolomite cement (D6)	-10.62	-2.2	--	--

Table 2

Dolomite type	Reservior rock type	Occurrence in thin-section	Morphology	Crystal size	Habit	Sedimentary facies	CL color
Dolomudstone (D1)	Crystalline dolomite reservoir	Dolomite crystal	Planar-e to planar-s micrite-fine to medium-crystalline	5-20μm	Replacing calcite, burrows filling	Lagoon, tidal flat	Dull red to red
Dolomicrite （D2）	Crystalline dolomite and breccia reservoir	Dolomite crystal	Planar-e to planar-s micrite-fine to medium-crystalline	5-20μm	Replacing calcite	Restricted lagoon and sabkha	Very dull red
Fabric-retentive dolomite (D3)	Reef reservoir	Reef framework	Planar-e to planar-s micrite-fine crystalline	10-40μm	Replacing calcite	Reef facies	Dull red
	Grain stone reservoir	Grain				Shoal facies	
Fabric-obliterative dolomite (D4)	Reef and grain stone reservoir	Reef and grain	Planar-s to nonplanar-a , medium- to coarse- crystalline	50-200μm	Replacing calcite, filling vugs	Reef facies	Dull red to red
		Reef and grain	Planar-s to nonplanar-a , medium- to coarse- crystalline		Replacing calcite, filling vugs	Shoal facies	
Medium to coarse dolomite cements (D5)	Reef, grain stone reservoir	Cement	Planar-e, planar-s to nonplanar-a, and Limpid euhedral	50-500μm	Filling primary porosity, vugs and fractures	Reef, shoal and platform facies	Red to orange
Saddle dolomite cements (D6)	Reef, grain stone reservoir	Cement	nonplanar-a and saddle	300-2000μm	Filling vugs and fractures	Reef, shoal and platform facies	Orange

Table 2 continued

Timing	Size of aqueous inclusions	$^{87}Sr/^{86}Sr$	$\delta^{18}O$ VPDB	Temperature	Salinity and dolomitization water	Dolomitization models
Penecontemporaneous	--	--	-6‰ to -5‰	20-25°C	Sea water (~3.5 wt%)	Microbial dolomitization
Penecontemporaneous	--	0.7088 - 0.7108	-6.5‰ to less than -3‰	30-35°C	Brine (~18.6 wt%)	Sabka and reflux dolomitization
Penecontemporaneous to shallow burial	< 2μm	0.7088 - 0.7093	-6.5‰ to -6‰	30-35°C	Brine (~18.6 wt%)	Reflux dolomitization
Shallow burial			-7.5‰ to -6.5‰	40°C	Sea water (~3.5 wt%)	Sea water dolomitization
Penecontemporaneous to shallow burial	4-10μm	0.7088 - 0.7097	-6.5‰ to -5.5‰	30-35°C	Brine (~18.6 wt%)	Reflux dolomitization
Medium to deep burial			-8‰ to -7‰	90-130°C	Brine (6 to 20 wt% NaCl)	Burial dolomitization
Deep burial to uplift	4-10μm	0.7093 - 0.7100	-9‰ to -8‰	90-130°C	Brine (6 to 20 wt% NaCl)	Burial dolomitization
Deep burial to uplift during hydrothermal events	6-12μm	0.7087 - 0.7091	-12‰ to -9‰	90-170°C	Brine (10 to 26 wt% NaCl)	Hydrothermal dolomitization

-- data not tested or unavailable